NASA TM-77083

NASA TECHNICAL MEMORANDUM NASA TM-77083

CONTRIBUTION TO THE AERODYNAMIC STUDY OF WINGS AND PROPELLERS

Maurice Menard

Translation of "Contribution a l'etude Aerodynamique de L'aile et de l'helice", Ministere de l'Air, Institut Aerotechnique de Saint-Cyr, Paris, France, Publications Scientifiques et Techniques 262, 1952, pp. 1-61.

NATIONAL AERONAUTICS AND SPACE ADMINISTRATION
WASHINGTON, DC 20546 JUNE 1983

STANDARD TITLE PAGE

1. Report No. NASA TM-77083	2. Government Accession No.	3. Recipient's Catalog No.
4. Title and Subtitle CONTRIBUTION TO THE AERODYNAMIC STUDY OF WINGS AND PROPELLERS		5. Report Date June 1983 6. Performing Organization Code
7. Author(s) Maurice Menard		8. Performing Organization Report No. 10. Work Unit No.
9. Performing Organization Name and Address SCITRAN Box 5456 Santa Barbara, CA 93108		11. Contract or Grant No. NASw 3542 13. Type of Report and Period Covered Translation
12. Sponsoring Agency Name and Address National Aeronautics and Space Administration Washington, D.C. 20546		14. Sponsoring Agency Code

15. Supplementary Notes

Translation of "Contribution a l'etude Aerodynamique de L'aile et de l'helice", Ministere de l'Air, Institut Aerotechnique de Saint-Cyr, Paris, France, Publications Scientifiques et Techniques 262, 1952, pp. 1-61.

16. Abstract

Various problems regarding the aerodynamics of lifting wings are solved. Two methods are proposed for replacing the wing, both involving "viscous" edge vortices. The applications give results which agree well with experiments. Two new methods are also proposed for calculating propellers based on the vortex model consisting of an edge vortex and a "viscous" hub vortex.

17. Key Words (Selected by Author(s))	18. Distribution Statement		
	unclassified and unlimited		
19. Security Classif. (of this report) Unclassified	20. Security Classif. (of this page) Unclassified	21. No. of Pages 80	22. Price

CONTRIBUTION TO THE AERODYNAMIC STUDY OF WINGS AND PROPELLERS*

Maurice Ménard and M. A. Toussaint

PREFACE

In order to develop an experimental method to study the aerodynamic functioning of profiles of propeller blades, M. Ménard first solved various problems about the aerodynamics of lifting wings.

First of all, he proposes a calculation method for the corrections caused by lateral boundary layers for "between panels" experiments, using the logarithmic law for the velocity distribution. In boundary layers and for the correlation variation of the circulation over a section of the experimental wing, he calculates the local induced angles and the average induced angles for this wing section. In this way, we obtain the corrections to be applied to the unit lift curves in order to extrapolate them for infinite length. Various applications perfectly justify the use of these corrections which occur for "between panel" tests. After this, M. Ménard makes an important and original contribution to the calculation of finite span wings. He proposes two methods of replacing the wing which both involve "viscous" edge vortices. This new model seems to represent real edge vortices very well. The applications made for the median section of the wings, and those for any other sections, give results which agree well with experiments, especially as far as the "edge effect" is concerned for the distribution of the lift force over the span of rectangular wings.

---

* Aero Technical Institute at Saint-Cyr, France. Scientific and Technical Publication of the Air Ministry. No. 262. (1952).

For the experimental study of the aerodynamic functioning of the profiles of a propeller blade, M. Ménard considered and developed a method of measuring the local aerodynamic incidence. This method consists of measuring the aerodynamic pressures at 3 points located close to the leading edge of the blade profile. The transmission of these pressures to micro-manometers required a "ceiling rotating joint" having 3 compartments.

Once the aerodynamic incidence of these various profiles of a blade are known and the characteristics of the same profiles for infinite span are known, one can calculate the radial distribution of the traction and coupling coefficients. By integrating this, one obtains the global coefficients for various values of $\gamma = \frac{V}{nD}$. The results calculated in this way agree well with the global measurements made with a balance.

Finally, M. Ménard proposed two new methods for calculating propellers based on the vortex model consisting of an edge vortex and a "viscous" hub vortex.

The application of these methods to the particular case of a propeller shows good agreement between the calculated and measured induced velocities.

In conclusion, it is obvious that the work of M. Ménard will interest aerodynamicists in laboratories and in study offices. In closing, I would like to confirm that I appreciated the collaboration at the Saint-Cyr Aero Technical Institute.

A. Toussaint,
Professor at the Scientific Faculty, Director of the Aero Technical Institute

TABLE OF CONTENTS

		Page
	Chapter I	5
	General Remarks	
	Chapter II	
	Study of an experimental infinite aspect ratio	
I.	Definition	7
II.	Theoretical study of the pseudo-plane flow	7
III.	Calculation of the aerodynamic characteristics of a wing placed in a pseudo-plane flow	22
IV.	Experimental configuration	25
V.	Presentation of results	28
	Chapter III	
	Theory of a wing with finite span	
I.	Summary of the Prandtl theory	41
II.	Calculation of induced velocities (Glauert method [6])	42
	Chapter IV	
	New methods for calculating the aerodynamic characteristics of a wing with finite span (Introduction of the viscosity of the ambient fluid)	
I.	General remarks	49
II.	Distribution of velocity in a vortex in a viscous fluid	51
III.	System of replacement no. 1 for a finite span wing	52
IV.	Replacement system no. 2 for a finite span wing	60
V.	Use of the replacement system no. 2 for the study of the influence of lateral boundary layers on tests between panels	71

/i

(Chapters V and VI are not included in this translation) /ii

Chapter I

/1*

GENERAL REMARKS

Modern calculation methods for propellers use the principles described by Joukowski [1] in 1912.

At this time, the calculation methods were based on the application of theorems of momentum and the moment of the momentum. These are theorems which allow one to define the values of the force and the couple of the propeller.

Joukowski attributes additional axial, radial and rotational velocities near the propeller to vortices, the existence of which was demonstrated by Flamm.

I. Propeller with arbitrary circulation distribution

In this case, the model of the vortex system used by Joukowski consists of the following:

a) radial vortices tied to the blade located in the propeller rotation plane;

b) free vortices which depart from the blade and roll up into solenoids.

The circulation of the vortex tied to the blade is defined as a function of the local lift coefficient, the relative resultant velocity to which the profile is subjected, and the length of the profile chord at the radius under consideration:

$$\Gamma = C_z \frac{Wl}{2};$$

Γ, circulation;

C_z, local lift coefficient;

W, resulting velocity at the radius under consideration;

*Numbers in margin indicate pagination of foreign text

l, chord of the profile.

Motion is assumed to take place in a perfect fluid, and the drag coefficient does not appear in this theory.

II. Propeller with constant circulation distribution /2

Joukowski gives a constant value of Γ_o to the bound vortex. The vortex sheet which makes up the wake of the propeller is replaced by an axial vortex having circulation Γ_o or 2 Γ_o (two-blade propeller) and a vortex at the tip of the blade with circulation Γ_o which rolls up into a solenoid.

The velocity induced by an element of the vortex of given length is defined by the Biot and Savart electromagnetic induction law.

For propellers with arbitrary circulation distribution, Joukowski points out the difficulty involved in calculating the values of induced velocity for any radius of a propeller using three helicoidal vortices.

In order to avoid this difficulty, the number of blades is increased indefinitely. This allows one to define average induced velocities for any radius of the propeller blades.

This calculation of the induced velocities allows one to define the angle of attack of the propeller for any section under consideration. This section is supposed to have the characteristics of an infinite span wing (same chord) calculated for the same aerodynamic incidence.

By indefinitely increasing the number of propeller blades, Joukowski substitutes a fictitious flow for the real flow which has on the average the properties which are comparable with those of

real flow.

III. Extension of the Joukowski theories

The theories derived from the Joukowski theory can be separated into two categories:

a) theories which use an infinite number of blades.

This involves a continuous vortex distribution. The induced velocities at radius r have a constant value along a circumference of radius r (average induced velocities).

A correction has to be applied in order to take into account the finite number of blades of the real propeller.

b) theories which use a finite number of blades.

This is proceeded by a calculation of the velocities induced at a given point of the blade by vortex strips which emanate from the blade and roll up into solenoids. The induced velocities have, therefore, been determined and are called "local" velocities.

/3

PURPOSE OF THE PRESENT STUDY

Numerous calculation methods for propellers have been proposed. The comparison with experiments shows that for propellers operating at high similitude $\frac{V}{n\ D}$ values, these methods provide sufficiently accurate approximations . It seems that there is a large disagreement between theory and experiment when the propellers operate at small values of $\gamma = \frac{V}{n\ D}$.

The purpose of this study is to research measurement procedures which will allow the determination of experimental conditions of aerodynamic operation of profiles which are used for propeller blades with a good degree of approximation. For this purpose, two

$$\frac{dT}{dr} = \frac{dR_z}{dr}\cos\varphi - \frac{dR_x}{dr}\sin\varphi$$

$$= p\,\frac{\rho}{2}\,W^2\,l\,(C_z\cos\varphi - C_x\sin\varphi),$$

$$\frac{dQ}{dr} = r\left(\frac{dR_x}{dr}\cos\varphi + \frac{dR_z}{dr}\sin\varphi\right)$$

$$= p\,\frac{\rho}{2}\,W^2\,l\,(C_x\cos\varphi + C_z\sin\varphi),$$

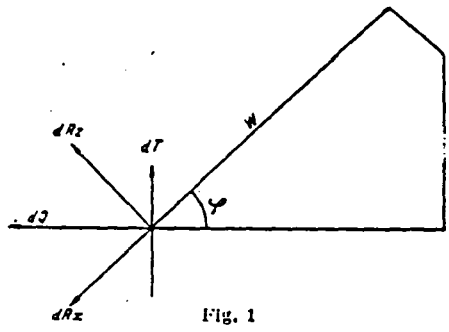

Fig. 1

measurement methods were used:

- measurement of an average velocity
- direct measurements on the blade.

I. Measurement of average velocity

This is an an anemometric study of the blowing of a propeller, a study which was performed with the usual measurement procedures (directional probe).

II. Direct measurements on the blade

Let us consider a propeller blade profile located at radius r; the resultant of the forces applied to this profile is equal to the geometric sum of lift and drag.

Let W be the resulting velocity over the blade at the radius under consideration. We can write:

$$dR_z = \frac{\rho}{2}\,C_z\,W^2\,l\,dr,$$

$$dR_x = \frac{\rho}{2}\,C_x\,W^2\,l\,dr.$$

In Figure 1, it is possible to describe the traction and the elementary couple for radius r.

The relationship between the angle ϕ and the geometric step angle θ of the propeller is:

$$\phi = \theta - i;$$

i = incidence of the profile under consideration.

The angle ϕ, incidence i and resulting velocity W determine the operational conditions of the propeller.

MEASUREMENT OF THE INCIDENCE AND THE VELOCITY

Let us consider a wing profile placed in a flat stream in a wind tunnel. Over this profile, we measured the pressure at three points. The pressure differences between two of these points and the third point (Δp_1 and Δp_2) are proportional to the square velocity of the flow at infinity and at the aerodynamic incidence angle of the profile.

Since we have a system of equations with two unknowns, it is possible to determine the aerodynamic incidence of the profile and the velocity at infinity, under the condition that we have first made pressure tap measurements. We use this procedure in order to determine the aerodynamic incidence and the velocity resulting at various radii of a propeller blade.

In order to measure these pressure taps, we constructed a wind tunnel with a flat rectangular test section in which we wish to directly measure the pressure taps over the blade. But the variation of the chord and the twist of the blade, for a section subjected to the flow, made these measurements inaccurate (variation of the circulation along the stand).

Under these conditions, we then studied pressure taps over a cylindrical wing with a constant chord and which had no twist, in order to construct a propeller having the same base profile. The lift of this wing was measured by integration of the pressure along the chord (median section). The slope of the unit curve of lift determined under these conditions was too small. This showed that

the fictitious equivalent aspect ratio obtained for plane flow (flat wind tunnel) did not have the characteristics of an experimental infinite aspect ratio, obtained between panels and with a geometric aspect ratio of 8.66 (special measurements performed in the median section of the wing).

We tried to establish the causes of this anomaly. From this, we then studied the influence of boundary layers which developed along wind tunnel walls for plane flow tests.

It seemed to us to be necessary for possible application to propeller blade measurements to know the influence of the aerodynamic flow field curvature close to a wing having finite span (curvature due to the presence of induced velocities which vary along the chord of the profile).

In the thesis of M. Carafoli, we note the difficulty encountered by the author when trying to superimpose the diagrams of pressure measured in the median section of wings having varying aspect ratio (diagrams reduced to the same aerodynamic incidence). This document led us to use a new model for the vortex system of a wing with finite span.

/5

The new replacement system proposed allowed us to do the following:

a) calculate the distribution of the circulation, along the span of a wing having finite aspect ratio;

b) to obtain the superposition of the diagrams for the median section of different finite aspect ratio wings, taking into account the field curvature. This was also done for wings tested between panels and which had different geometric aspect ratios;

c) to correct measured pressures measured over the propeller blade (in order to take into account the field curvature);

d) to establish a new vortex model which is simple and which can be used to calculate a propeller.

Chapter II

/7

STUDY OF AN EXPERIMENTAL INFINITE ASPECT RATIO

I. Definition

In aerodynamics, one usually considers a cylindrical wing which is displaced perpendicular to its generators in a perfect fluid. Under these conditions, one has realized a theoretically infinite aspect ratio. The motion of the fluid around the wing is called "two-dimensional" or "plane flow". The flow is identical for all sections perpendicular to the wing generators.

It is very difficult to realize a wing whose geometric aspect ratio is very high (pseudo-infinite). All of the experimental configurations built to obtain a correct experimental infinite aspect ratio attempt to make the results independent of the geometric aspect ratio of the wing under study.

Among all of these realizations, we will now consider the one used at the Saint-Cyr Air Technical Institute (test between panels).

Professor Toussaint [2] has stated that infinite experimental aspect ratio is difficult to establish in the wind tunnel for the following reason:

- The transverse distribution of velocity between the two parallel walls of a wind tunnel is not flat. Along these walls, boundary layers develop. The motion of the fluid particles around the profile under consideration is not uniform along the generators of the wing under study. Therefore, we no longer have a "plane" flow.

II. Theoretical study of the pseudo-plane flow

Let us consider a wing A of span L having a constant profile along the span and not warped placed between two parallel walls PP'

of a wind tunnel through which a fluid current flows of velocity V. We will study the influence of boundary layers existing on the walls PP' on the aerodynamic characteristics of the wing (Figure 2).

For edge regions of the wing located inside the boundary layers B, C, the velocity of the flow is no longer V but it is U.

/8

The pseudo-plane experimental flow will be considered as being equivalent to the linear juxtaposition of the following:

a) a theoretical plane flow for which the aerodynamic incidences are the same over the the entire span of the wing (geometric incidence referred to the direction of 0 width of the profile)

b) a flow caused by the velocities induced by the system of free vortices coming from edge regions where the circulation is variable due to the fact that the velocity U is different from V.

The juxtaposition of these two flows leads to a system of the integral-differential type for determining the velocities induced along the span of the wing. In order to simplify the calculations, we assume that the variation of the circulation along the span of the wing is only caused by the transverse gradient of the velocity which exists in the boundary layer. This amounts to ignoring the action of flow b).

Let:

i, geometric incidence in the median plane;
$\frac{dc_z}{di}$, slope of the unit curve of lift for the median section;
l, chord of the wing.

The circulation in the median section has the following value:

(1) $$\Gamma_0 = i \frac{dC_z}{di} \frac{V_0}{2} l.$$

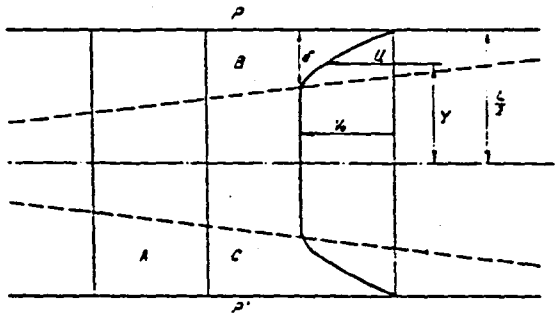

Fig. 2

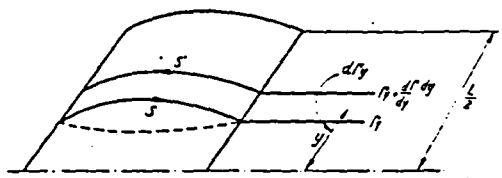

Fig. 3

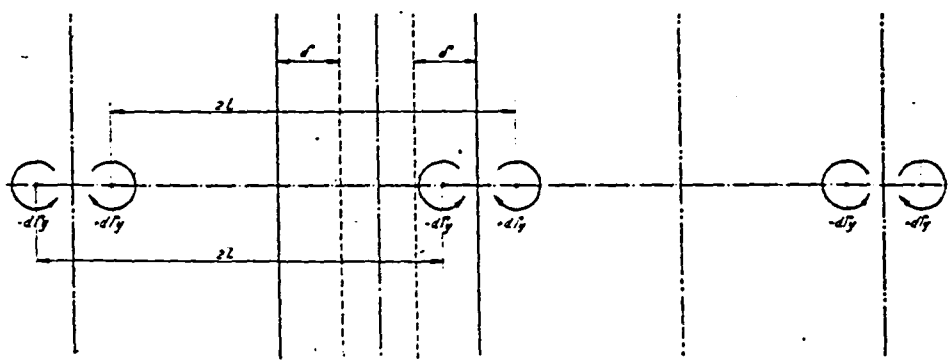

Fig. 4

The circulation in the plane having ordinate value y is equal to:

$$\Gamma_y = i \frac{dC_z}{di} \frac{u}{2} l. \tag{2}$$

1. Diagram of the equivalent vortex system

Just like in the case of a wing whose span is finite (therem of Prandtl), we assume a single vortex placed at the focus of the wing, a vortex which has the same circulation as the real wing.

/9

The attached vortex has the same transverse dimension as the wing and the same circulations as the real wing at the same points at each of the points.

Let us consider the extremity of the wing over which a circulation gradient is established (Figure 3).

In the plane with the ordinate y, the circulation is Γ_y. In the plane y + dy, the circulation is:

$$\Gamma_y + \frac{\partial \Gamma_y}{\partial y} dy.$$

For the planes with ordinates y and y + dy, therefore, we have the circulation:

$$\Gamma_y - \left(\Gamma_y + \frac{\partial \Gamma_y}{\partial y} dy\right) = -\frac{\partial \Gamma_y}{\partial y} dy = d\Gamma_y.$$

This elementary circulation will be considered as the circulation of the free vortex emanating from the profile at this point.

The collection of the free vortices will constitute a plane sheet.

Also, the flow exists between walls and it is necessary to take into account the stresses imparted to the flow by the walls.

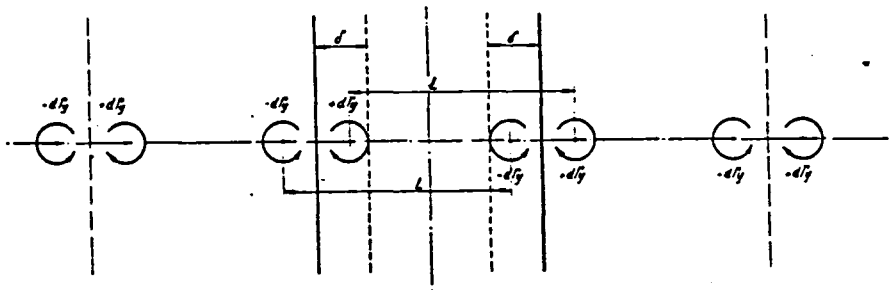

Fig. 5

In the replacement vortex system, we represent these stresses by infinite rows of vortices with alternate orientations.

If we consider the free vortex with circulation $-d\Gamma_y$ emanating from the profile in the plane y, the vortex system which takes into account the presence of the walls is the one described by Figure 4.

By symmetry, it is obvious that at a point with an ordinate -y, a free vortex with the circulation $+d\Gamma_y$ will detach. Taking into account this remark, the diagram of the vortex system becomes the one shown in Figure 5.

We are dealing with an infinite row of vortices with alternate orientations $\mp d\Gamma_y$ of step L and with ordinate origins of $\pm y$.

The complex potential for the row $+d\Gamma_y$ is:

$$f_1(z) = -i\frac{d\Gamma_y}{2\pi}\left\{\operatorname{Log}(z+y) + \sum_1^\infty \operatorname{Log}[(z+y)^2 + m^2L^2]\right.$$

For the row $d\Gamma_y$, we have

$$f_2(z) = +i\frac{d\Gamma_y}{2\pi}\left\{\operatorname{Log}(z-y) + \sum_1^\infty \operatorname{Log}[(z-y)^2 - m^2L^2]\right.$$

For the two rows, the complex potential is then:

$$F(z) = -i\frac{d\Gamma_y}{2\pi}\left\{\operatorname{Log}\frac{(z+y)[(z+y)^2+L^2][(z+y^2)+2L^2][\ldots][(z+y)^2+m^2L^2]}{(z-y)[(z-y)^2-L^2][(z-y^2)-2L^2][\ldots][(z-y)^2-m^2L^2]}\right.$$

By making an expansion, we obtain the formula of M. Villat:

$$F_z = -i\frac{d\Gamma_y}{2\pi}\operatorname{Log}\frac{\sin\frac{\pi}{L}(z+y)}{\sin\frac{\pi}{L}(z-y)}.$$

The complex velocity corresponding to this will be:

$$dw = \frac{dF(z)}{dz} = -i\frac{d\Gamma_y}{2\pi}\frac{\pi}{L}\left[\operatorname{cotg}\frac{\pi}{L}(z+y) - \operatorname{cotg}\frac{\pi}{L}(z-y)\right]$$

$$= i\frac{d\Gamma_y}{L}\frac{\sin\frac{2\pi y}{L}}{\cos\frac{2\pi y}{L} - \cos\frac{2\pi z}{L}}.$$

At a point with an ordinate Y, the complex velocity is reduced to the vertical component and its value is given by: /11

(4) $$dv = \frac{d\Gamma_y}{L}\frac{\sin\frac{2\pi y}{L}}{\cos\frac{2\pi y}{L} - \cos\frac{2\pi Y}{L}}.$$

In the calculation we have assumed that the free vortices were infinite in the two directions. But here we only have semi-vortices (emanating from the wing) and by symmetry, the expression (4) has to be divided by 2:

(5) $$dv = \frac{d\Gamma_y}{2L}\frac{\sin\frac{2\pi y}{L}}{\cos\frac{2\pi y}{L} - \cos\frac{2\pi Y}{L}}.$$

The induced velocity resulting from the point Y will be equal to the sum of the velocities induced by all of the free vortices and their images at point Y, that is:

$$v = \int_{\frac{L}{2}-\varepsilon}^{\frac{L}{2}} dv.$$

2. Representation of velocities in the boundary layer

a) Friction law

The formula generally used for friction of a flow over a flat plate without a longitudinal gradient of static pressure is the one given by Prandtl:

$$\frac{\tau_0}{\rho V_0^2} = \frac{0{,}01255}{\left(\frac{V_0 \delta^{xx}}{\nu}\right)^{\frac{1}{4}}}, \tag{6}$$

with

$$\delta^{xx} = \int_0^{\delta} \frac{u}{V}\left(1 - \frac{u}{V}\right) dy.$$

Let us apply the theorem of momentum to the boundary layer. We have:

$$\frac{\tau_0}{\rho V_0^2} = \frac{d\,\delta^{xx}}{dx}. \tag{7}$$

This expression allows one to express the friction as a function of Reynolds number. If we consider the equations (6) and (7), we have:

$$\frac{d\,\delta^{xx}}{dx} = \frac{0{,}01255}{\left(\frac{V_0 \delta^{xx}}{\nu}\right)^{\frac{1}{4}}},$$

/12

or:

$$\frac{d\,\delta^{xx}}{dx}(\delta^{xx})^{\frac{1}{4}} = \frac{0{,}01255}{\left(\frac{V_0}{\nu}\right)^{\frac{1}{4}}}.$$

Let us integrate this expression between the limits 0 and x. We have:

$$\frac{4}{5}(\delta^{xx})^{\frac{5}{4}} = \frac{0{,}01255\,x}{\left(\frac{V_0}{\nu}\right)^{\frac{1}{4}}},$$

from which we find

$$\frac{\delta^{xx}}{x} = \frac{0{,}036}{(\mathcal{R}x)^{\frac{1}{5}}}, \tag{8}$$

with $$\mathcal{R}x = \frac{V_0 x}{\nu},$$

and finally $$\frac{\tau_0}{\rho V_0^2} = \frac{0{,}0288}{(\mathcal{R}x)^{\frac{1}{5}}};$$

b) distribution of the velocities in the boundary layer

In the boundary layers which developed over a flat plate subjected to a turbulent flow without longitudinal static pressure gradient, the velocity profiles are similar, that is, they can be represented by a single curve.

We can represent the velocity profile in the boundary layer by using a law of the following form:

(9) $$\frac{u}{V_0} = 1 + K_1 \operatorname{Log}\left(\frac{y}{\delta}\right).$$

For the following calculations, this leads us to the following:

$$\delta^x = \int_0^{\delta} \left(1 - \frac{u}{V_0}\right) dy$$

(10) $$= \int_0^1 K \operatorname{Log}\left(\frac{y}{\delta}\right) d\left(\frac{y}{\delta}\right) = K_1 \delta.$$

$$\delta^{xx} = \int_0^{\delta} \frac{u}{V_0}\left(1 - \frac{u}{V_0}\right) dy$$

$$= \delta \int_0^1 - \left(1 + K_1 \operatorname{Log}\frac{y}{\delta}\right) K_1 \operatorname{Log}\left(\frac{y}{\delta}\right) d\left(\frac{y}{\delta}\right),$$

(11) $$\delta^{xx} = K_1 (1 - 2 K_1) \delta.$$

/13

If we consider equations (10) and (11), we can see that it is possible to obtain by graphical integration the quantities δ^x and

δ^{xx} if we have an experimental distribution of velocity in the boundary layer. This allows us to determine the value of the coefficient K_1 introduced in formula (9). M. Michel [3] shows that with this coefficient it is possible to determine a thickness δ_L which is not the ordinate where $u = V_o$ but which determines in a more accurate manner the values of δ^x and δ^{xx} by associating them with the values of K_1. The friction values and the values of flow rate are therefore represented better.

Experimentally, we have noted a small deviation between the thicknesses δ_L and δ.

We can relate the shape parameter H to the coefficient K_1:

$$H = \frac{\delta^x}{\delta^{xx}} = \frac{1}{1 - 2K_1}.$$

Our representation of velocity (9) can be written as:

$$\frac{u}{V_0} = 1 + \frac{H - 1}{2H} \operatorname{Log} \frac{y}{\delta_L}.$$

For a flat plate without a longitudinal static pressure gradient in turbulent flow, the value of the shape parameter H is equal to 1.3, that is:

$$K_1 = 0{,}116.$$

We finally find the following as a representation law of velocity in the boundary layer:

(12) $$\frac{u}{V_0} = 1 + 0{,}116 \operatorname{Log}\left(\frac{y}{\delta}\right).$$

3. Introduction of the law $\frac{u}{V_0} = 1 + K_1 \operatorname{Log} \frac{y}{\delta}$ as a representation of the velocity in the boundary layer

It is useful to define the transverse circulation gradient in order to find the velocity induced at an arbitrary section of the wing.

We have seen that it can be written in the form:

$$d\Gamma_y = \frac{\partial \Gamma}{\partial y} dy.$$

Formulas (1) and (2) of paragraph II result in the following:

(13)
$$\frac{\Gamma_0}{\Gamma_y} = \frac{V_0}{u}, \qquad \Gamma_y = \Gamma_0 \frac{u}{V_0}.$$

/14

In the preceding paragraph we have seen that it was possible to adapt formula (9) as a velocity law in the boundary layer from which we find

(14)
$$\Gamma_\xi = \Gamma_0 \left(1 + K_1 \operatorname{Log} \frac{\xi}{\delta}\right).$$

By considering equations (8) and (11), we find

$$\frac{\delta}{\delta^{xx}} = \frac{1}{K_1 (1 - 2 K_1)}, \qquad \frac{\delta}{\delta^{xx}} = 11{,}22 \qquad \text{with} \qquad K_1 = 0{,}116,$$

(15)
$$\delta = \frac{11{,}22 \times 0{,}036}{\left(\frac{V_0 x}{\nu}\right)^{0{,}2}}.$$

This latter formula allows one to calculate the thickness of the boundary layer at the measurement point x (this is only true in the case where we assume turbulent flow over a flat smooth plate without any static pressure gradient in the longitudinal direction).

Let us consider figure 6; in the formula (14), ξ will be defined by:

$$\xi = \frac{L}{2} - y.$$

The equation (14) can be written as:

(16)
$$\Gamma_\xi = \Gamma_0 \left(1 + K_1 \operatorname{Log} \frac{\frac{L}{2} - y}{\delta}\right).$$

The transverse circulation gradient is:

(17)
$$d\Gamma_y = \frac{\partial \Gamma}{\partial y} dy = K_1 \Gamma_0 \frac{dy}{\left(y - \frac{L}{2}\right)}.$$

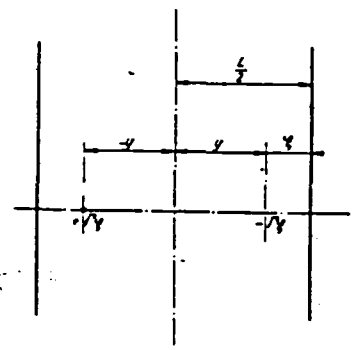

Figure 6

We have found in paragraph 1 that the velocity induced at a point with ordinate Y by a free vortex and its images was:

$$dv = \frac{d\Gamma_y}{2L} \frac{\sin \frac{2\pi y}{L}}{\cos \frac{2\pi y}{L} - \cos \frac{2\pi Y}{L}}. \tag{18}$$

By relating equations (17) and (18), we have

$$dv = \frac{K_1 \Gamma_0}{2L} \frac{\sin \frac{2\pi y}{L}}{\left(\cos \frac{2\pi y}{L} - \cos \frac{2\pi Y}{L}\right)} \times \frac{dy}{\left(y - \frac{L}{2}\right)}. \tag{19}$$

The resultant velocity induced at the point with ordinate Y by vortices "from the boundary layer" and their images will be given by: /15

$$v_y = \frac{K_1 \Gamma_0}{2L} \int_{\frac{L}{2}-\delta}^{\frac{L}{2}} \frac{\sin \frac{2\pi y}{L}}{\left(\cos \frac{2\pi y}{L} - \cos \frac{2\pi Y}{L}\right)} \frac{dy}{\left(y - \frac{L}{2}\right)}, \tag{20}$$

and the integration can be performed graphically.

The velocity diagram at the ordinate point will be the one shown in Figure 7. We can rewrite:

$$\frac{v_Y}{V_y} = \operatorname{tg} \delta i_y \cong \delta i_Y$$

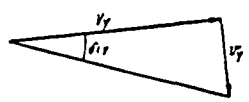

Figure 7

V_y (axial velocity at distance Y from the axis).

Two cases have to be considered:

a) the ordinate Y is located inside the boundary layer, the velocity of the flow is equal to V_o and the local induced angle can be written as given by (20) and by using $\Gamma_0 = C_z \frac{V_0 l}{2}$, we have:

$$\delta i_{Y_0} = \frac{K_1 C_z l}{4L} \int_{\frac{L}{2}-\delta}^{\frac{L}{2}} \frac{\sin \frac{2\pi y}{L}}{\left(\cos \frac{2\pi y}{L} - \cos \frac{2\pi Y}{L}\right)} \frac{dy}{\left(y - \frac{L}{2}\right)}; \tag{21}$$

b) the ordinate Y is located inside the boundary layer, the velocity of the flow at this point α is U, and the local induced angle becomes:

$$\delta i_y = \frac{v_Y}{U} = \frac{K_1 C_z V_0 l}{4 L U} \int_{-\frac{L}{2}}^{+\frac{L}{2}} \frac{\sin \frac{2\pi y}{L}}{\left(\cos \frac{2\pi y}{L} - \cos \frac{2\pi Y}{L}\right)} \frac{dy}{\left(y - \frac{L}{2}\right)}$$

(22)

$$= \frac{1}{\frac{u}{V_0}} \frac{K_1 C_z l}{4 L} \int_{-\frac{L}{2}}^{+\frac{L}{2}} \frac{\sin \frac{2\pi y}{L}}{\left(\cos \frac{2\pi y}{L} - \cos \frac{2\pi Y}{L}\right)} \frac{dy}{\left(y - \frac{L}{2}\right)}.$$

It is possible in equation (22) to use the logarithmic representation of the velocity in the boundary layer:

$$\delta i_u = \frac{K_1 C_z l}{1 + K_1 \operatorname{Log}\left(\frac{\frac{L}{2} - Y}{\delta}\right)} \int_{-\frac{L}{2}}^{+\frac{L}{2}} \frac{\sin \frac{2\pi y}{L}}{\left(\cos \frac{2\pi y}{L} - \cos \frac{2\pi Y}{L}\right)} \frac{dy}{\left(y - \frac{L}{2}\right)}.$$

(23)

We will define an average induced angle as follows: /16

(24)

$$\Delta i = \frac{1}{L} \int_{-\frac{L}{2}}^{+\frac{L}{2}} \delta i_y \, dy.$$

III. Calculation of the aerodynamic characteristics of a wing placed in a pseudo-plane flow

We have defined an angle induced at the section Y of a wing placed in a pseudo-plane flow. Because of this induced angle, the usual reference axis system (directions parallel and perpendicular to the velocity direction at infinity upstream) will be changed.

In Figure 8, we see that the resultant of the forces applied is no longer perpendicular to V_y but perpendicular to V. We then have:

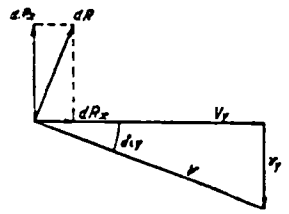

Fig. 8

$$dR_z = dR\cos\delta i_y$$
$$= \rho V_y \Gamma_y dy \cos\delta i_y$$
$$= \rho V_y \Gamma_y dy \cong \rho V \Gamma_y dy,$$
$$dR_z \cong dR.$$

Thus, the modification of the lift can be considered as small. On the other hand, as far as the drag is concerned, we show a very substantial increase which can be written as:

$$dR_x = dR\sin\delta i_y = \rho \Gamma_y V_y \sin\delta i_y dy$$
$$= \rho \Gamma_y v_y dy \cong \frac{v_y}{V_y} dR_z,$$

since:

$$dR_x = \frac{v_y}{V_y} dR_z,$$

(25)
$$\frac{v_y}{V_y} = \delta i_y,$$
$$dR_x = \delta i_y dR_z.$$

We can determine the induced local resistance coefficient:

(26)
$$dR_z = C_z \frac{\rho}{2} V^2_y dy\, l;$$

(27)
$$dR_x = C_x \frac{\rho}{2} V^2_y dy\, l;$$

using (26), (27) and (25), we have:

(28)
$$C_{x_i} \frac{\rho}{2} V^2_y l\, dy = \delta i_y C_z \frac{\rho}{2} V^2_y l\, dy,$$
$$C_{x_i} = C_z \delta i_y.$$

/17

In paragraph II, we have defined an average induced angle from an examination of the distribution of induced local angles along the span of the wing. The induced angle had the following value:

(29)
$$\Delta i = \frac{1}{L}\int_{-\frac{L}{2}}^{+\frac{L}{2}} \delta i_y dy.$$

The lift and drag coefficients measured with aerodynamic balances are average coefficients (since we weigh the entire wing). In Figure 9, we show the unit curves of lift. I represents the unit

curve of lift measured with the balance.

We have seen that for a given value of the lift coefficient, the reference axis position changes. For a lift coefficient value of $C_Z = C_{Z_0}$, the aerodynamic incidence is therefore not α but $\alpha - \Delta i$. In order to obtain the corrected unit curve of lift, it is sufficient to plot the following curve:

$$C_z = f(\alpha - \Delta i).$$

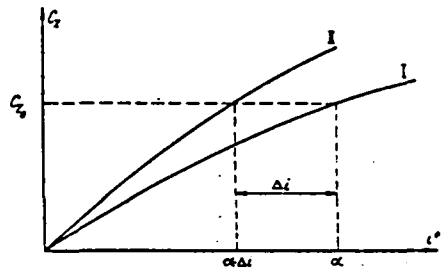

Fig. 9

Before we have seen that there was an increase in the "induced" drag. The drag coefficient measured with a balance can be written as:

$$C_{x_B} = C_{x_i} + C_{x_{ind}}.$$

The indices:

B = balance

C = corrected

i = induced

have been defined.

The C_{x_i} is equal to:

(30)
$$C_{x_i} = C_{x_B} - C_{x_0}.$$

In order to make corrections to the unit drag curves, $C_X = F(i)$ measured with the balance, one has to take into account the fact that there is an induced drag and that the geometric incidence of the wing is reduced by an amount Δi (average induced angle).

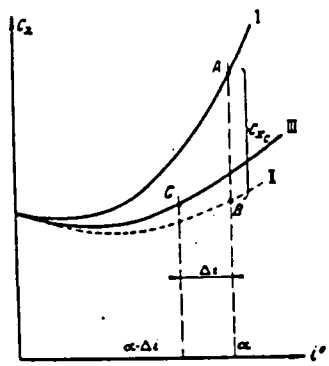

Fig. 10

In Figure 10, we show successive corrections to be applied to unit curves of drag measured with the balance. The distance AB represents the C_x induced for a value of C_z corresponding to the incidence α. In order to take into account the average induced angle, it is necessary to attribute a new value C_x derived from (30) to the aerodynamic incidence $(x - \Delta i)$. The distance BC therefore represents $(x - \Delta i)$.

/18

Remark. When we measured the drag coefficient by the wake method, we only measured the value C_{x_c}. In order to make corrections, it is necessary to take into account the local incidence variation due to the local induced angle δi_y (measurement plane).

IV. Experimental configuration

1. Determination of lateral boundary layer characteristics

Before each series of tests, we made velocity measurements in the lateral boundary layers of the wind tunnel. We made these measurements essentially at the location where the focus of the wing was located. In order to perform these measurements, we used a total pressure tube whose extremity was flattened and the sides were defined as follows (interior): 0.10 mm x 2.5 mm; exterior: 0.5 mm x 3.5 mm). This total pressure curve was closed off by a carriage which allowed displacements of 0.2 mm.

2. Measurement of aerodynamic forces (lift)

We used three measurement procedures:

a) Brass tubes inserted in the profile.

The profiles were made of walnut. In the profiles we engraved grooves parallel to the generators using a mill. Brass tubes, 0.7 x 1.5 mm, were introduced in these grooves and were glued using strong

glue. We provided for a correct surface of the profile by using cellulose mastic in order to cover up the roughnesses caused by milling of the profile.

The pressure probe holes had a diameter of 0.5 mm and were arranged over the same section of the wing in order to avoid measurement errors introduced by a fast variation of the induced angle along the span.

b) Pressure measurements on the profile using a licking probe.

For this purpose, we used a probe having special characteristics. We did not wish to use the carriage which supports a licking probe because this procedure has a certain number of disadvantages. For example, it is luminous and there is risk of introducing local perturbations in the circulation around the profile being measured. This makes it difficult to measure in regions around the leading edge and around the trailing edge of the wing.

The measurement probe is a modern type as far as its shape of its extremities are concerned. In Figure 11, we show a diagram showing the shape of the probe support:

- AB, pressure probe which can pivot around axis B;
- BC, small rod which can turn around the axis C;
- at B and C, reference springs which make the part AB be parallel to the profile and therefore parallel to the flow.

/19

During the calibration of this probe, we noted that there was an interaction between the part BC and the part AB. When the distance BC' is greater than 20 times the diameter of the stem DC, indications of the probe are independent of the position of BC.

With this measurement device, it was possible to measure pressures over wing profiles from the leading edge up to 20 mm from the trailing edge.

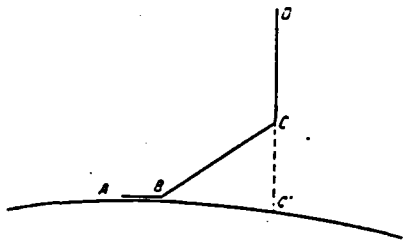

Fig. 11

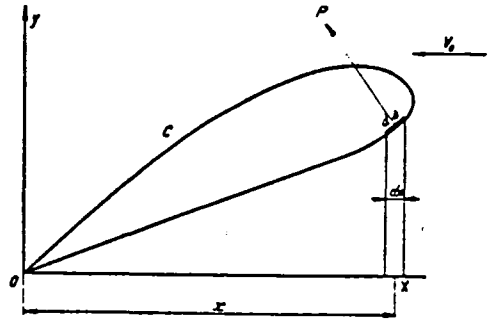

Fig. 12

The part DC was connected to a device which allowed the translation of the probe parallel to the chord of the profile studied.

The calibration curve of the probe is shown in plate 1.

The measurement of the pressures over the wing allowed us to determine the lift of this wing. With consideration of Figure 12, the lift of the wing can be represented by the integral:

$$P = \int_c p\, ds \cos\alpha$$
$$= \int_c p\, dx,$$

which is an integral which extends over the entire contour of the profile. In order to carry out the integration, we construct the pressure diagram as a function of the abscissa OX of the projection of the measurement point on the flow direction with a flow speed of V_o.

c) Measurement of the lift using an aerodynamic balance

In wind tunnel no. 1 at Saint-Cyr, there is a pseudo-rectangular test section with a width of 0.78 meters and a height of 2 meters. The wing was placed between the panels and is connected by means of a wire network to a type Denis-Gruson aerodynamic balance. The lateral play allowed between the wing and the panel is 2 mm.

3. Measurement of aerodynamic forces (drag)

We determined the drag of the wings tested either by using an aerodynamic balance or by the wake method. In the latter case, we started with measuring the velocity in the wakes of the wings in order to find the loss in momentum of the fluid close to the profiles under consideration. We used formulas established by Jones which allow one to determine the drag coefficient from static pressure measurements and total pressure measurements performed upstream and downstream of the wing: /20

H_o, total pressure at infinity upstream;

H_1, total pressure in the measurement plane;

V_o, velocity at infinity upsream:

$$\Delta H = H_1 - H_o$$

We have:

$$C_{x_r} = \frac{1}{l} \int_0^y \frac{\Delta H}{\frac{\rho}{2} V_0^2} (1 - K)\, dy :$$

0 and y are wake limits;

K is the correction coefficient of Jones, taking into account the differences in static pressure between infinity upstream and the measurement point.

V. Presentation of results

In the experiments we allowed the various quantities which intervene in the correction formulas of the preceding paragraphs to vary:

1. Variation of the characteristics of lateral boundary layers

We constructed a wind tunnel with a rectangular cross-section (0.050m x 0.50m). The test section length is 1 meter (see Figure 13 and photograph Figure 14).

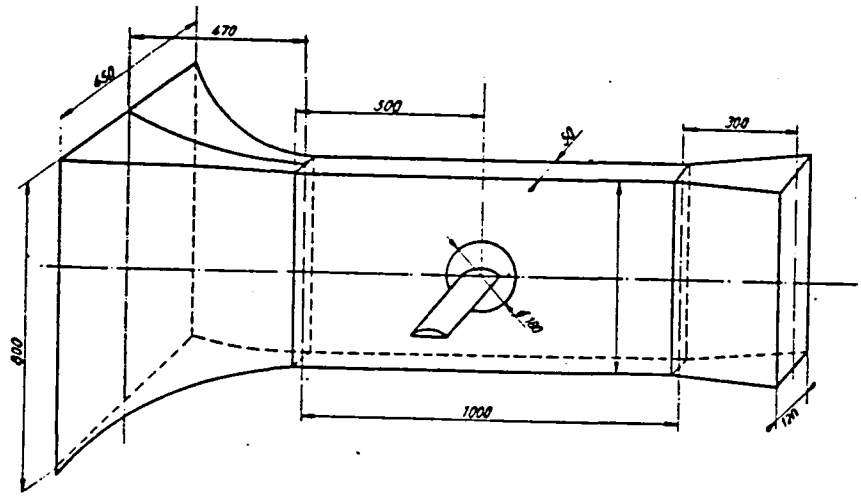

Figure 13

We made the longitudinal static pressure gradient 0 by divergence of the small dimension walls. On the large side of the wind tunnel, we drilled orifices which allowed us to introduce side plates carrying the impression of the profile under study.

/21

The static pressures were measured in the median section of a wing with a chord of 132 mm (Figure 15) for different incidence angles. This allowed us to determine the corresponding C_z values.

Figure 14

The characteristics of the lateral boundary layers were changed with the surface state of the collector.

The curves (plate 2) show the velocity distributions in the boundary layers at the measurement point. The wind tunnel collector was rough or smooth.

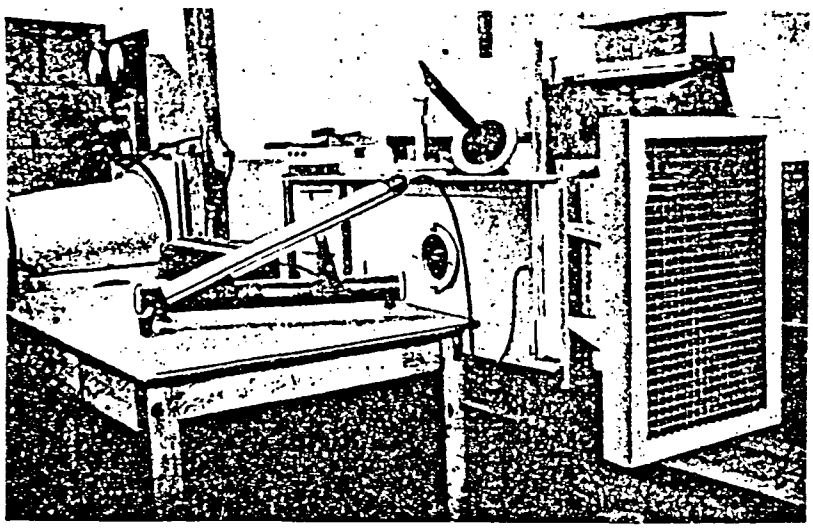

Figure 15

The lateral boundary layers have the following characteristics:

a) rough collector:

$$\delta_L = 16.5 \text{ mm}, \qquad K_1 = 0.115;$$

b) smooth collector:

$$\delta_L = 12.8 \text{ mm}, \qquad K_1 = 0.128$$

The curves $C_z = F(i)$ for the two configurations are shown in plate 3 and the corresponding values are given in Tables 1 and 2:

TABLE 1. Rough collector

$i°$	$-4°$	$-2°$	$2°$	$4°$	$6°$	$8°$	$10°$
$100\ C_z$	$-27,5$	$-11,1$	$+18,6$	$+34,4$	$+50,3$	$+65,3$	$+78,7$

TABLE 2. Smooth collector

/22

$i°$	$-3°,2$	$-1°,10$	$4°,8$	$6°,8$	$8°,8$
$100\ C_z$	$-21,5$	$-4,7$	42,5	60	74,7

The induced local angle for the median section is determined from:

$$\delta i_{Y=0} = \frac{K_1 C_z l_0}{4L} \int_{\varepsilon}^{\frac{L}{2}} \frac{\sin \frac{2\pi y}{L}}{\left(\cos \frac{2\pi y}{L} - 1\right)}, \qquad \frac{dy}{\left(y - \frac{L}{2}\right)} = \frac{K_1 C_z l_0}{4L} \int_{\varepsilon}^{\frac{L}{2}} \operatorname{cotg} \frac{\pi y}{L} \frac{dy}{\left(y - \frac{L}{2}\right)},$$

for a lift coefficient value taken equal to 100 C_Z = 50.

The calculated induced angles are the following:

- rough collector: 2.59°
- smooth collector: 2.07°

The slopes of the unit curves C_Z = f(i) corresponding to this are:

- rough collector: 0.0757;
- smooth collector: 0.0815

The slopes of the curve C_Z = f(i) after corrections are equal to:

- rough collector: 0.1245;
- smooth collector: 0.1233

In plate 3 we show the unit curves. We can see that between the curves obtained after corrections for the boundary layer effect and the other curve, there is a slight deviation which is on the order of magnitude of the experimental errors.

2. Variations of the geometric aspect ratio of the profile

For these test, we used a Clark Y type profile with a relative thickness of 18% and a cord of l = 0.090 m. We measure the pressures in the median section of the wing profile for two very different geometric aspect ratios. The wing is placed in a flat wind tunnel with a section of 0 .050m x 0.50m and then in a Lelarge wind tunnel with plane flow having a section of 0.78m x 1.50m. In the two cases

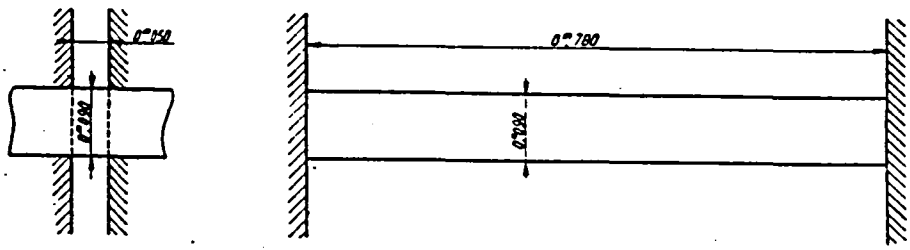

Figure 16

considered, the wing traverses the wind tunnel from one wall to the other without lateral play (Figure 16).

/23

The geometric aspect ratios of the wing for two test conditions are the following:

- 0.050m x 0.50m wind tunnel

$$\lambda_o = 0.55;$$

- 0.78m x 1.50m wind tunnel

$$\lambda_g = 8.66$$

The height of the plane flow is different in the two cases and it is necessary to make a correction to take into account the limited height of the fluid channel. We will use an experimental correction of M. Toussaint:

$$\frac{C_{z_{h=\infty}}}{C_{z_h}} = \frac{1}{1 + 0{,}863\,\frac{l^2}{h^2}};$$

h, height of the fluid channel;

l, chord of the profile;

$C_{z_{h=\infty}}$, value of the lift coefficient for an infinite height of the fluid channel;

C_{z_h}, value of the lift coefficient for a height h of the fluid channel.

The lift coefficients derived from pressure measurements for the Clark Y profile are given in Tables 3 and 4 and the corresponding $C_z = F(i)$ curves are shown in plate 4:

TABLE 3. — $\lambda_g = 0,55$

$i°$	— 8	— 4°	— 2°	0°	2
100 C_z	4	36	53,5	69	85,5

TABLE -4. — $\lambda_g = 8,66$

$i°$	— 8°	— 6°	— 4°	— 2°	— 0°,50	1	4	6°	8	10°
100 C_z	7,5	29	49	68,5	81,5	99	122	135	145,5	158,7

The characteristics of the boundary layers for the two tests are the following:

- 0.050m x 0.50m wind tunnel:

$$\delta_L = 12.8 \text{ mm} \qquad K_1 = 0.128$$

- 0.78m x 1.50 m wind tunnel:

$$\delta_L = 50.8 \text{ mm} \qquad K_1 = 0.12$$

/24

The slopes of the unit curves $C_z = F(i)$ are:

- 0.050m x 0.50 wind tunnel:

$$\frac{dC_z}{di} = 0.0807$$

- 0.78m x 1.50m wind tunnel:

$$\frac{dC_z}{di} = 0.103$$

The corrections to be made to the above coefficients are the following in order to take into account the limited height of the fluid channel:

- 0.050m x 0.50m wind tunnel:

$$\frac{C_{z_{corr}}}{C_{z_A}} = \frac{1}{1,028} = 0,973;$$

- 0.78m x 1.50m wind tunnel:

$$\frac{C_{z_{corr}}}{C_{z_A}} = \frac{1}{1,0031}.$$

In the latter case, the correction can be ignored.

For a value of the coefficient 100 C_z = 50, the angle induced in the median section of the wing is equal to:

0.050m x 0.50m wind tunnel:

$$\delta i_{y=0} = 1^{\circ},41;$$

0.78m x 1.50m wind tunnel:

$$\delta i_{y,0} = 0^{\circ},019.$$

The slopes of the unit curves corrected for the "boundary layer effect" are:

0.050m x 0.50 wind tunnel:

$$\frac{dC_z}{di} = 0,1017;$$

0.78m x 1.50m wind tunnel:

$$\frac{dC_z}{di} = 0,103.$$

We can see on the one hand that we have practically realized an infinite experimental aspect ratio in the Lelarge wind tunnel. The angle induced for the median section is very small. Also, the unit curves for lifts obtained after correction have slopes which are independent of the geometric aspect ratio of the wing.

25

3. Determination of the global forces applied to the wing

In order to perform these tests, we used wind tunnel no. at Saint-Cyr. The profile study had the following characteristics:

- profile HM_{12}, chord l = 0.600m; relative thickness 12%, biconvex; geometric aspect ratio λ_y = 1.3.

The unit lift curve of this profile was determined by measuring pressures in the median section. The unit drag curve was determined by measuring the wakes (median section). The global forces which apply to the wing were measured using an aerodynamic balance.

a) Lift measurements

The curve which gives the velocity profile in the lateral boundary layers is represented in plate 5. The determination of the characteristics of the lateral boundary layers gives:

$$\delta_L = 31.5 \text{ mm} \qquad K_1 = 0.1125.$$

Using graphic integration, it is possible to determine the variation of the induced angle along the semi-span of the wing using formula (23). Plate 6 shows this variation for a value of 100 C_z = 100.

The average value of the induced angle corresponding to this is equal to

$$\Delta i = 1.15°$$

The calculated induced angle for the median section is equal to:

$$\delta i_{y=o} = 0.15°$$

In Table 5, we give the values of the coefficients C_z obtained by integration of the pressures measured in the median section of the wing for various incidences:

TABLE 5

I°	0°	2°	4°	6°	8°	10°
100 C_z	15,5	36	57,3	78,7	99	114,5

In Table 6, we show the lift coefficients and drag coefficients measured with the balance:

TABLE 6

I°	— 3°,60	— 1°,60	0°,50	2°,50	4°,50	6°,60	8°,60	10°,60
100 C_z	— 19,1	— 2,65	19,1	39	57,9	77	95	112.2
100 C_x	1,21	1,05	1,055	1,43	2,02	2,67	3,68	5

/26

If we consider plate 6, we can see a difference between the slopes of the lift curve determined from pressure measurements on the profile and those derived from balance measurements.

For 100 C_z = 100, the angular variation of the reference axis system corresponding to the slope changes gives an induced angle equal to 1°. It should be noted that the unit lift curve measured from pressure measurements in the median section is not the unit curve corresponding to an infinite experimental aspect ratio. The calculation shows that there is a local induced angle for the section under consideration which is equal to:

$$\delta i_{y=o} = 0.15°$$

In order to correct the slope of the lift curve determined with the balance, it is necessary to take into account the change in the angular position of the reference axis system equal to

$$\Delta i = 1° + \delta i_{y=o} = 1.15°$$

This angle is exactly equal to the average induced angle determined by calculation.

Therefore, the curve $C_z = f(i)$ resulting from global measurements from the balance amounts to the curve $C_z = f(i)$ for infinite experimental conditions.

Remark. We can determine the equivalent fictitious aspect ratio obtained for tests between panels in wind tunnel no. 1 for a wing with a chord of 0.600 m, by assimilating the wing between the panels into a wing having a finite span with aspect ratio λ_f such that:

$$\Delta i = \frac{C_z}{\pi \lambda} \times 57{,}3;$$

for 100 C_z = 100, we have:

$$\Delta i = 1°{,}15 = \frac{57{,}3}{\pi \lambda_f},$$

$$\lambda_f = \frac{57{,}3}{3{,}61} = 15{,}9;$$

b) Drag measurements

In Table 7, we show the values of C_x measured by the wake method for the median section of the wing.

TABLE 7

I°	— 2°	0°	2°	4°	6°	8°
100 C_x	0,88	0,78	0,78	0,82	1,055	1,45

Plate 8 shows a substantial difference between the curve determined from the balance and the one determined by the wake method. We have to correct the values measured with the balance in order to take into account the induced drag, and this corresponds to:

$$C_{x_c} = C_z \Delta i.$$

/27

In Table 8, we show the values of measured drag coefficients measured with the balance, after correction for the induced drag:

TABLE 8

I°	— 2°	0°	2°	4°	6°	8°
100 C_{x_c}	1,07	1	1,03	1,203	1,5	1,9

In plate 8, we show that the deviation found between the curve determined with the wake method and that obtained by weighing is considerably reduced after corrections are made. The disagreement between the two tests is in part caused by the fact that the model was connected to the balance with a number of wires which results in a turbulent flow over a large part of the wing. The measurements of momentum loss were performed in the median section of the wing, a location where the flow is not perturbed. It is, therefore, normal that the drag coefficient determined by this latter method would be less than the one found with the balance (Figure 17).

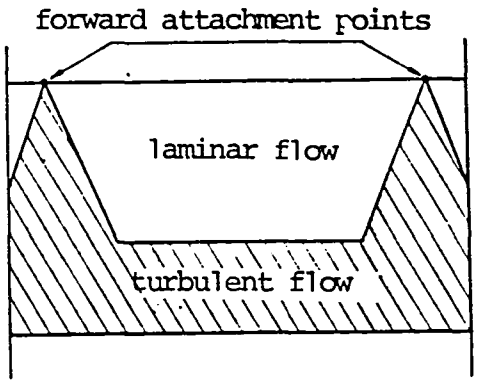

Figure 17

Also, Mr. Carafoli showed that the edge perturbations come from the lateral play which exists between the wing and the panels. This produces an increase in the drag coefficient which is a function of the play.

In plate 9, we show the polar relative to Cx determined by the wake method associated with values of C_z corresponding to an infinite experimental aspect ratio. We also show those found from balance measurements. Finally, we show the polar from balance measurements which were corrected for the "boundary layer effect".

The moment coefficient of the wing was determined from balance measurements and also from pressure measurements performed in the median section of the wing. The results of these measurements are given in Tables 9 and 10:

TABLE 9

I°	— 3,6	0°,50	2°.50	4°,50	6°,60	8°,60	10°.60
100 C_{M_B}	5	10	15	19,6	24,3	28,7	32,3

/28

TABLE 10

I°	2°	4°	6°	8°	10°
100 C_{M_P}	13,8	19,45	24,4	29	33

Plate 10 shows the curves $C_M = f(i)$ for these tests.

In order to obtain the corrected $C_M = f(i)$ curve, from moment measurements with the balance, it is sufficient to shift the position of the reference axes as in the case of the unit lift curves.

4. Tests of Mr. Carafoli [4]:

In work performed before the work of Mr. Carafoli, various authors tried to obtain a correct experimental infinite aspect ratio, by avoiding the short circuiting of pressures on the top side and the bottom side. Mr. Carafoli tried to eliminate this effect by allowing the edge play between the wind tunnel wall and the wing to vary. The extrapolation of the characteristics obtained in this way for zero play should then furnish the results where the edge effect is ignored. Nevertheless, Mr. Carafoli found a difference in slope between the curves determined from the balance (extrapolated for zero play) and those obtained by pressure measurements in the median wing section.

The difference noted between the reference indices relative to these tests is equal to 0.50° for 100 $C_z = 100$.

Using formula (15), we determine the thickness of the boundary layer to the right of the wing focus. By introducing this value in formula (23), we can determine the vararіation of the angle induced along the span of the wing and we therefore find an average induced angle.

Tests performed by Mr. Carafoli for wings with aspect ratios between $\lambda_g = 2$ and $\lambda_g = 8$ and referred to infinite aspect ratio (Prandtl method) show a substantial disagreement with tests performed between panels.

In plate 11, we show tests and also the polar measured for plane flow and corrected for the "boundary layer effect".

5. Tests of Mr. Girerd [5].

Mr. Girerd tried to obtain a correct experimental infinite aspect ratio by using guard tips having the same profile as the portion measured and which follows the incidence variations of it. The tips were selected sufficiently long in order that the perturbations induced by the transverse velocity gradient in the boundary layer could be avoided and could not be felt at the wing.

The angle induced by the "boundary layer vortices" was calculated for a certain number of points along the span of the wing. The variation of this angle induced along the measured part is shown in plate 12. An average induced angle was derived from this curve. By assimilating the wing into a wing with finite aspect ratio λ_f, it is possible to calculate the equivalent fictitious aspect ratio obtained in the test of Mr. Girerd:

/29

$$\Delta i = \frac{C_z}{\pi \lambda_f} 57{,}3 \qquad \text{for} \qquad C_z = 100,$$

Δi_m for the measured sec. $\Delta i_m = 0°{,}08,$

$$\lambda_f = \frac{57{,}3}{\pi \times 0{,}03} = 238.$$

Conclusions:

The calculation method used may be imperfect but allows one to obtain corrections which agree well with experiments.

The results obtained are practically independent of the geometric aspect ratio of the wings used. Under these conditions, it can be stated that the aerodynamic characteristics determined after the "boundary layer" corrections have been made are those which correspond to an infinite experimental aspect ratio.

Chapter III /31

THEORY OF A WING WITH FINITE SPAN

I. Summary of the Prandtl theory

Let us consider flow around a wing with finite aspect ratio.

Aerodynamic phenomena to which the wing is subjected are not studied for the period in which the flow regime at velocity V_o is established. The motion of the fluid is assumed to be permanent.

The simplified hypotheses of the linear Prandtl theory are the following:

- An aircraft wing can be assimilated into a system of vortices making up the wall of the wing and connected to it and another system of vortices, "free vortices", which make up an infinite sheet (a sheet which develops in the wake of the wing). The bound vortices are parallel to the general direction of the span. For wings for which the span is large with respect to the depth, it is assumed that the velocity induced by the free vortex sheet is constant along the depths of the wing at a given section. The elementary force of this section is proportional to the sum of the elementary circulations distributed over the section.

Therefore, one can concentrate all of the circulations at their center of gravity. The geometric location of these points is a single line which can replace the wing. The lifting surface of the wing is therefore replaced by a "lifting line".

The free vortices detach at the trailing edge perpendicular to the span. These vortex strips essentially follow the direction of the general flow. A flat vortex sheet extends from the lifting line to infinity downstream.

The vortex intensity of a strip of width dy is equal to the variation of the circulation along this lifting line at this point:

$$\Gamma_y = \frac{\partial \Gamma}{\partial y} dy.$$

The free vortices induce velocity distributed along the span. These are induced velocities which modify the position of the reference axes (position which was tied to the direction of the air flow at infinity upstream).

/32

The change in the direction of the reference axis results in a component of resistance (induced drag) with the following value:

$$dR_x \cong \frac{w}{V_0} dR_z.$$

The aerodynamic global coefficients of the wing are:

$$R_z = \rho V_0 \int_{-\frac{L}{2}}^{+\frac{L}{2}} \Gamma \, dy,$$

$$R_x = \rho \int_{-\frac{L}{2}}^{+\frac{L}{2}} \Gamma w \, dy = R_{x_i}.$$

II. Calculation of induced velocities (Glauert method [6]):

Let us consider a vortex strip of intensity Γ_y which escapes at the trailing edge of the wing at a distance y from the median section (Figure 18):

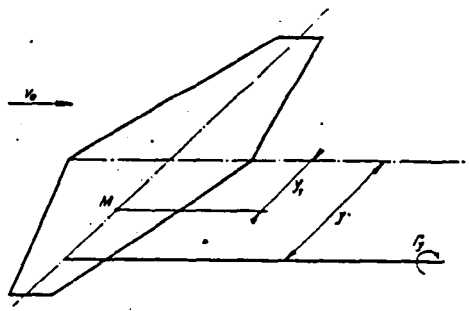

Figure 18

The velocity induced at the point M located at a distance of y_1 from the median section and for a strip which extends to infinity downstream is:

$$dw_1 = -\frac{1}{2}\frac{1}{2\pi}\frac{\Gamma_y}{(y-y_1)} = -\frac{1}{4\pi}\frac{\partial\Gamma}{\partial y}\frac{dy}{(y-y_1)}.$$

The velocity induced at the point M for all strips emanating from the wing is:

$$w_1 = -\frac{1}{4\pi}\int_{-\frac{L}{2}}^{+\frac{L}{2}}\frac{\partial\Gamma}{\partial y}\frac{dy}{(y-y_1)}.$$

/33

The angle induced in the section under consideration is:

$$\varphi_1 \cong \frac{w_1}{V_0} = \frac{1}{4\pi V_0}\int_{-\frac{L}{2}}^{+\frac{L}{2}}\frac{\partial\Gamma}{\partial y}\frac{dy}{(y-y_1)}.$$

We are dealing with an integral-differential type of system. Glauert gave a solution.

The circulation over the wing is expressed in the form of a trigonometric series by setting:

$$y = -\frac{L}{2}\cos\psi \qquad \text{and} \qquad dy = \frac{L}{2}\sin\psi\, d\psi.$$

L is the span of the wing. ψ is a variable whose limits are 0 and π for values of y equal to $-\frac{L}{2}$ and $\frac{L}{2}$:

$$\Gamma = 2LV_0\sum_1^{\infty} A_n \sin n\psi,$$

from which

$$d\Gamma = 2LV_0\sum_1^{\infty} n\,A_n\cos n\psi\, d\psi$$

and

$$w = \frac{1}{4\pi}\int_{-\frac{L}{2}}^{+\frac{L}{2}}\frac{\partial\Gamma}{\partial y}\frac{dy}{y-y_1}$$

(1)

$$= \frac{2LV_0}{4\pi}\int_0^{\pi}\frac{\sum_1^{\infty} nA_n\cos n\psi\, d\psi}{\frac{L}{2}(\cos\psi-\cos\psi_1)} = \frac{V_0}{\pi}\int_0^{\pi}\frac{\sum_1^{\infty} A_n\cos n\psi\, d\psi}{\cos\psi-\cos\psi_1}.$$

The resolution of the integral (1) was given by Glauert. One obtains

$$\frac{w}{V_0} = \frac{1}{\sin\psi} \sum_1^{\infty} nA_n \sin n\psi. \tag{2}$$

The theoretical circulation at a point of a wing with infinite aspect ratio is:

$$\Gamma = 4\pi a V_0 \sin i_a \cong \pi l (1 + \eta e) V_0 i_a : \tag{3}$$

a, radius of the generating circle;
i_a, aerodynamic incidence of the wing;
l, chord of the profile;
n, coefficient which varies between 0.6 and 0.75;
e, relative thickness of profile.

/34

The aerodynamic incidence at a given section of the wing with finite span, is

$$i_a = i_g - \varphi \cong i_g - \frac{w}{V_0}, \tag{4}$$

where ϕ is the angle induced at the section under consideration.

By combining equations (3) and (4), we have:

$$\Gamma \pi l (1 + \eta e) V_0 \left(i_g - \frac{1}{4\eta V_0} \int_{-\frac{L}{2}}^{+\frac{L}{2}} \frac{\partial \Gamma}{\partial y} \frac{dy}{y - y_1} \right). \tag{5}$$

In (5) we replace the integral by its value (1):

$$\Gamma = \pi l (1 + \eta e) V_0 \left(i_g - \sum_1^{\infty} \frac{nA_n \sin n\psi}{\sin\psi} \right),$$

where

$$A_n = a_n i_g.$$

The lift component has the following expression:

$$R_z = \rho V_0^2 L^2 \int_0^{\pi} \sum_1^{p} A_n \sin n\psi \sin\psi \, d\psi$$

$$= \frac{\rho}{2} V_0^2 \pi L^2 A_1.$$

The unit lift coefficient is: $$C_z = \frac{R_z}{\frac{\rho}{2} V_0^2 S} = \pi A_1 \frac{L^2}{S} = \pi A_1 \lambda$$

$$= \frac{\pi A_1 \lambda i}{i} = \pi a_1 \lambda i;$$

for the slope of the unit lift curve we have:

$$\frac{dC_z}{di} = \pi a_1 \lambda.$$

By comparing the theoretical lift curves for infinite aspect ratio and aspect ratio λ, we have:

$$\frac{C_{z\lambda}}{C_{z\infty}} = \frac{\pi a_1 \lambda}{2\pi (1 + \eta e)} = \frac{\lambda}{2(1 + \eta e)} \cdot \frac{A_1}{i},$$

or

$$i_\infty = \frac{C_z}{2\pi (1 + \eta e)} \qquad \text{and} \qquad i_\lambda = \frac{C_z}{\pi a_1 \lambda};$$

/35

The global induced angle has the following value

$$\varphi_g = i_\lambda - i_\infty = \frac{C_z}{\pi \lambda} \left(\frac{1}{a_1} - \frac{\lambda}{2(1 + \eta e)} \right),$$

$$\varphi_g = \frac{C_z}{\pi \lambda} (1 + \tau).$$

The induced resistance component can be expressed by:

$$R x_1 = \rho \int_{-\frac{L}{2}}^{+\frac{L}{2}} \Gamma w \, dy = \rho V_0^2 L^2 \int_0^{\pi} \left(\sum A_n \sin n\psi \right) \left(\sum n A_n \sin n\psi \right) d\psi$$

$$= \rho V_0^2 L^2 \frac{\pi}{2} \sum_1^p n A_n^2 = \frac{\rho}{2} V_0^2 \pi L^2 \sum_1^p n A_n^2$$

$$= \frac{\rho}{2} V_0^2 L^2 A_1 \sum_1^p \frac{n A_n^2}{A_1^2} = R_z A_1 (1 + \delta),$$

with

$$1 + \delta = \sum_1^p \frac{n A_n^2}{A_1^2} = \sum_1^p \frac{n a_n^2}{a_1^2}.$$

By using the unit drag coefficient, we find:

$$C_{x_i} = \frac{Rx_i}{\frac{\rho}{2} S V_0^2} = C_z A_1 (1 + \delta),$$

$$C_{x_i} = \frac{C_z^2}{\pi \lambda} (1 + \delta).$$

Applications to monoplane wings

a) Rectangular wing

The terms in the expansion of Γ have odd indices. Since the series is highly convergent, we can write:

$$\Gamma = 2 L V_0 \{ (A_1 \sin \psi + A_3 \sin 3\psi + A_5 \sin 5\psi + A_7 \sin 7\psi) \}.$$

We can select the following particular values:

$$\psi_1 = \frac{\pi}{8} = 22°,50, \qquad \psi_2 = \frac{\pi}{4} = 45°, \qquad \psi_3 = \frac{3\pi}{8} = 67°,50, \qquad \psi_4 = \frac{\pi}{2} = 90°,$$

corresponding to the values of $\frac{2y}{L}$:

$$\frac{2y}{L} = 0,924, \qquad 0,707, \qquad 0,383, \qquad 0.$$

/36

It is possible to determine the coefficients A_1, A_3, A_5, A_7. We can also say that:

$$\mu = \frac{Kl}{2L} = \frac{K}{2\lambda} = \frac{1}{\frac{2\lambda}{K}} \qquad \text{and} \qquad \mu i = \frac{C_z}{\pi \lambda} \left(\frac{\mu i}{A_1} \right),$$

$$1 + \delta = \frac{A_1^2 + 3 A_3^2 + 5 A_5^2 + 7 A_7^2}{A_1^2},$$

$$1 + \tau = \frac{2\lambda}{K} \left(\frac{\mu i}{A_1} - \frac{\pi}{4} \right),$$

$$\frac{\varphi_0}{\mu i} = \frac{A_1 - 3 A_3 + 5 A_5 - 7 A_7}{\mu i} \qquad \text{and} \qquad \frac{K'}{K} = \frac{\pi}{4} \left(\frac{A_1}{\mu i} \right).$$

In Table 1, we give the values of the coefficients defined above.

For the median section, we have:

TABLE 1

$\frac{\lambda}{K}$	$\frac{\lambda}{K_1}$	$\frac{\lambda}{1+\eta e}$	$\frac{A_1}{\rho l}$	$\frac{A_3}{\rho l}$	$\frac{A_5}{\rho l}$	$\frac{A_7}{\rho l}$	$\frac{K_1}{K}$	τ	δ	$\frac{z_0}{\rho l}$	$\frac{\rho l}{A_1}$
0	0,640	0	0	0	0	0	0	0	0	0	∞
0,10	0,747	0 314	0,171	0,002	~ 0	~ 0	0,134	0,013	~ 0	0,165	5,850
0,25	0,908	0,785	0,351	0,008	~ 0	~ 0	0,275	0,030	~ 0	0,327	2,850
0,50	1,175	1,57	0,541	0,025	~ 0	~ 0	0,425	0,065	0,006	0,466	1,850
0,75	1,449	2.355	0,660	0,042	~ 0	~ 0	0.518	0,09	0,012	0,534	1,513
1	1.705	3,14	0,748	0,060	0,009	0,0014	0,587	0,10	0.019	0,603	1,336
1,5	2,225	4.71	0,859	0,090	0,016	0.0027	0,675	0,14	0,034	0,649	1,165
2	2 750	6,28	0,928	0,115	0,023	0,0041	0,729	0,17	0.049	0,668	1,077
2.5	3,260	7,86	0,976	0,136	0,030	0.0055	0,767	0,20	0,063	0,680	1.025
3	3,780	9,43	1,011	0,154	0.036	0.0070	0,794	0,22	0,076	0,680	0.990
3,5	4.290	11,00	1,038	0,169	0,042	0,0084	0,815	0.24	0,088	0,680	0,965

$$\psi = \frac{\pi}{2} \sin\psi = 1,$$

$$\varphi_0 = A_1 - 3\,A_3 + 5\,A_5 - 7\,A_7$$
$$= i\,(a_1 - 3\,a_3 + 5\,a_5 - 7\,a_7),$$
$$\varphi_0 = iA.$$

The variations of these coefficients are shown in plate 13 as a function of $\lambda' = \frac{\lambda}{1+\eta e}$.

/37

Plate 14 shows the values of the coefficients A for various values of λ.

b) Wing with elliptical circulation distribution

The circulation is expressed by

$$\Gamma = \Gamma_0 \sqrt{1 - \left(\frac{2y}{L}\right)^2}.$$

Γ_0 is the circulation for the median section of the wing with $y = \frac{L}{2} \cos\psi$:

$$\Gamma = \Gamma_0 \sqrt{1 \cos^2 \psi} = \Gamma_0 \sin \psi = 2 L V_0 A_1 \sin \psi,$$

$$A_1 = \frac{\Gamma_0}{2 L V_0}, \qquad A_3 = 0, \qquad A_5 = 0, \qquad A_7 = 0.$$

The induced velocity has the following value:

$$w = \frac{V_0}{\sin \psi} A_1 \sin \psi = \frac{\Gamma_0}{2 L} = C^{te}.$$

Thus, the induced velocity along the span of a wing with elliptical circulation distribution is constant.

Chapter IV

/39

NEW METHODS FOR CALCULATING THE AERODYNAMIC CHARACTERISTICS OF A WING WITH FINITE SPAN

(Introduction of the viscosity of the ambient fluid)

I. General remarks

In the theory of Prandtl, it is assumed that the span of the wing is large with respect to its depth. The induced velocity induced by the free vortices is constant along the depth of the wing.

Let us consider Figure 19. The velocity induced by a vortex element of intensity of $d\Gamma$ and of length dl at a section M of a wing with a finite span varies along the depth of the wing. This velocity is defined by the electromagnetic Biot and Savart induction law:

$$dw = \frac{d\Gamma}{4\pi}\frac{dl\sin\alpha}{r^2};$$

Therefore, it is a function of the distance of the vortex element from the point under consideration.

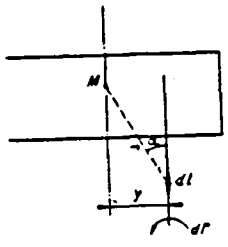

Figure 19

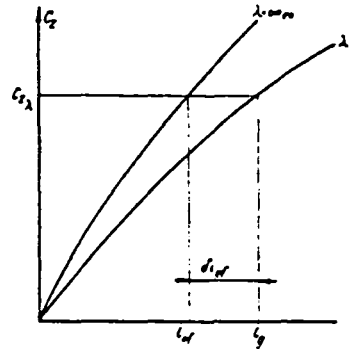

Figure 20

/40

Concentrating the elementary circulations of attached vortices at their center of gravity amounts to ignoring the fact that the velocity induced by the vortex strip varies along the chord of the wing.

We examined the results obtained by Mr. Carafoli about pressure measurements performed in the median section of finite span wings and with different aspect ratios (2 to 8).

In Figure 20, we show the curves $C_z = f(i)$ for an aspect ratio λ and infinite experimental aspect ratio. For the geometric incidence angle i_g and for an aspect ratio λ, we have a well defined value of C_{z_λ}. On the curve for the experimental infinite aspect ratio, the value of C_{z_λ} corresponds to an incidence angle i_{e_f} which can be related to i_g by means of:

$$i_{ef} = i_g - \delta i_{ef} \quad (a).$$

δi is the angle induced in the section under consideration.

We will introduce the term "effective incidence" and by this we mean the incidence angle defined by (a).

Mr. Carafoli drew plots of pressures for each orifice of the pressure taps as a function of the effective incidence angle. All of the diagrams should have been identical. The deviation found between the various curves increases as the aspect ratio decreases and as the orifices under consideration approach the leading edge of the wing.

Also, we found that for finite span wings with plane rectangular shapes, there is an increase in the lift near the edge borders, a phenomenon which is not represented by theories derived from the theory of Prandtl.

Finally, in experiments one finds two vortices which originate at the side edges of the wing. Certain authors assume that the sheet of fictitious free vortices introduced by Prandtl could be transformed into two edge vortices, assuming a rolling up of the free vortices, which occurs immediately at the trailing edge of the wing. It is difficult to take into account this rolling up in calculation.

We attempted to find replacement vortex systems for a wing with finite span by using the following experimental facts:

- presence of two edge vortices in the wake of the wing;
- edge vortices which do not have the properties of vortices in perfect fluids, and the fluid in which this occurs produces viscous motion.

Two systems of replacement for the finite span wing have been proposed. They have the following common features: The edge vortices have a circulation Γ'_o which we will define later on and they are established in a viscous fluid.

System 1

The elementary circulations of the attached vortices are concentrated at their center of gravity and make up a lifting line located essentially at the focus of the wing.

/41

System 2

At a given section, the elementary circulations of the attached vortices are distributed over the median line of the profile which confirms the theory of thin profiles.

II. Distribution of velocity in a vortex in a viscous fluid

Together with Mr. Villat [7], it is assumed that the velocity distribution law in a vortex in a viscous fluid is given by

(1) $$v = \frac{\Gamma'_0}{2\pi r}\left(1 - e^{-\frac{r^2}{4\nu t}}\right).$$

At the Aerotechnical Institute at Saint-Cyr, an experimental configuration allows one to measure the velocities in a physical vortex. Two small windmills A and B (Figure 21) driven by electrical motors M_1 and M_2 turn in the same direction and with equal velocity if possible.

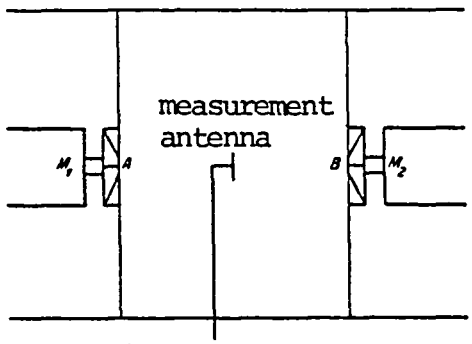

Figure 21

Velocity is measured at a section located at equal distances A and B which allows one to verify the curves obtained with those determined using equation (1). These curves are given in plate 15.

III. System of replacement no. 1 for a finite span wing

1. Hypotheses

The circulations of the attached elementary vortices are concentrated at the focus of the wing profile. The position of these points defines a lifting line with the same transverse dimensions as the real wing. The two edge vortices in a viscous fluid escape from the wing at the focus of the extreme profiles. They follow the general flow direction of velocity V and extend from the wing to infinity, and induce velocities in the wing plane.

/42

2. Determination of the circulation of the edge vortices

In order to calcuate the velocity induced at a section of the wing by edge vortices, it is necessary to determine their circulation.

We will first start with the evaluation of a circulation in the first approximation for all sections of the wing. For a wing whose depth of chord varies or for which there is warping, the circulation at a point of the lifting line is defined by

$$\Gamma'_y = C_{z_y} \frac{V_0 l_y}{2}$$

(2)
$$= i_g \left(\frac{dC_z}{di}\infty\right) \frac{V_0 l_y}{2} :$$

l_y, chord of the profile under consideration;
i_g, geometric incidence angle of the profile referred to the 0 lift direction;
$\frac{dC_z}{di}\infty$, slope of the unit lift curve of the profile under study for experimental infinite aspect ratio.

By using equation (2) we determine the distribution of the first approximation of circulation along the span of the wing. The maximum value achieved in this distribution defines the circulation Γ'_0 of the edge vortices.

For a wing with a constant profile and chord and which is not twisted (rectangular wing), the circulation of the lifting line is constant along the span and is equal to

$$\Gamma'_0 = C_z \frac{V_0 l}{2} = i_g \left(\frac{dC_z}{di}\infty\right) \frac{V_0 l}{2} :$$

i_g, geometric incidence of the profile referred to the 0 lift direction;
$\frac{dC_z}{di}\infty$, slope of the unit lift curve of the profile for infinite experimental aspect ratio;
V_0, translation velocity;
l, chord of the wing.

In this case, the circulation of the edge vortices is equal to the circulation which would exist at all sections of the wing if it had infinite experimental aspect ratio.

Thus, the determination of the circulation of the edge vortices is done by not considering the velocities which they induce on the wing.

3. Calculation of induced velocities

The velocity induced by a vortex in a viscous fluid at the point M located at a distance r_1 from this vortex is equal to the following according to (1):

$$v_1 = \frac{\Gamma'_0}{2\pi r_1}\left(1 - e^{-\frac{r_1^2}{4\nu t}}\right). \tag{3}$$

In the case of the wing, we are dealing with a semi-vortex. By symmetry, expression 3 has to be divided by 2; we then find:

$$v_1 = \frac{\Gamma'_0}{4\pi r_1}\left(1 - e^{-\frac{r_1^2}{4\nu t}}\right). \tag{4}$$

The resulting induced velocity at M (Figure 22) is equal to the sum of the induced velocities at this point by vortices 1 and 2.

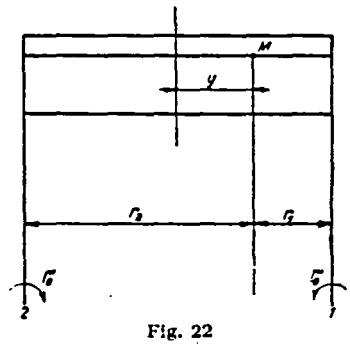

Fig. 22

Figure 22

The velocity induced by vortex 2 located at a distance r_2 from M, is equal to:

$$v_2 = \frac{\Gamma'_0}{4\pi r_2}\left(1 - e^{-\frac{r_2^2}{4\nu t}}\right), \tag{5}$$

so that the resulting induced velocity at M has the following value:

$$w = \frac{\Gamma'_0}{4\pi}\left[\left(\frac{1 - e^{-\frac{r_1^2}{4\nu t}}}{r_1}\right) + \left(\frac{1 - e^{-\frac{r_2^2}{4\nu t}}}{r_2}\right)\right]. \tag{6}$$

The velocity diagram at the point M is shown in Figure 23. The aerodynamic incidence of the local profile is modified by an induced angle, whose value at the ordinate point y is equal to:

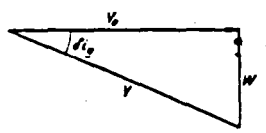

Figure 23

$$\frac{w}{V_0} = \operatorname{tg}\delta i_y \cong \delta i_y \cong \frac{\left(i_y \frac{dC_z}{di} \infty V_0 l\right)^{\max}}{2V_0 \times 4\pi}\left[\left(\frac{1 - e^{-\frac{r_1^2}{4\nu t}}}{r_1}\right) + \left(\frac{1 - e^{-\frac{r_2^2}{4\nu t}}}{r_2}\right)\right]. \tag{7}$$

In particular, for the median section of the wing, the induced angle has the following value:

(8) $$\delta i_{y=0} = \frac{\left(i_g \frac{dC_z}{di} \alpha \cdot \right)_{max}}{4\pi} \left(\frac{1 - e^{-\frac{L^2}{16 l}}}{\frac{L}{2}} \right).$$

/44

For the median section, we can see that the viscosity term can be ignored. $\lambda = \frac{L}{l}$, becomes:

$$\delta i_{y=0} = \frac{\left(i_g \frac{dC_z}{di} \alpha \, l\right)_{max}}{2\pi L};$$

in the case of rectangular wings $\lambda = \frac{L}{l}$, we have:

$$\delta i^0_{y=0} = 57{,}3 \frac{i_g \frac{dC_z}{di} \alpha}{2\pi\lambda},$$

(9) $$\delta i^0_{y=0} = A i_g. \qquad \frac{\delta i^0_{y=0}}{i_g} = A.$$

which is an expression that has an identical form as the one found by the Glauert theory.

4. Experimental verifications

a) Median section

First of all, we should mention the test performed at the Aero-Technical Institute of Saint-Cyr by Mr. Carafoli. These were done before pressure measurements over median sections of wings having variable aspect ratio (2 to 8). Also, he carried out measurements in the median section of a wing placed between panels. For these latter conditions, the correction formulas for the "boundary layer effect" established in Chapter II allow one to show that the equivalent fictitious aspect ratio obtained is practically equal with the infinite experimental aspect ratio.

If we have the curves $C_z = f(i)$ derived from pressure measurements in the median section of wings with aspect ratios (2 to 8)

and the curve $C_z = f(i)$ for the infinite experimental aspect ratio (pressures measured in the median section of a wing between panels) from deviations between these curves, it was possible for Mr. Carafoli to derive the corresponding induced angles. According to Figure 24, for a given value of C_z one can associate the effective incidence angle i_{ef}. The difference between the geometric incidence and the effective incidence is equal to the experimental induced angle:

Figure 21

$$\delta i_{ex} = i_g - i_{ef}.$$

In Figure 14, we show the variation of the experimental and induced angle determined by Mr. Carafoli as a function of aspect ratio λ of wings tested. The induced angle is expressed in the usual form:

$$\frac{\delta i_{ex}}{i_1} = A_{ex}.$$

/45

In plate 14, we show the curves of the variation of the various coefficients obtained from the measurements of Mr. Carafoli from the Glauert theory and our replacement system no. 1.

b) Distributions of lift along the span

The documents about the experimental distributions of lift along the span of wings with finite aspect ratio which we used do not all contain the aerodynamic characteristics of profiles of tested wings (lift angle 0 of profiles, experimental infinite aspect ratio slope). Therefore, this data was necessary in order to calculate the characteristics of wings. We proceeded as follows:

- In Figure 25, 1 is the unit curve of lift for the profile located in the median section of a rectangular wing with aspect ratio λ. 2 shows the unit curve of lift relative to infinite experimental aspect ratio. We can write:

(10) $$i_g = \frac{C_{z_\lambda}}{\frac{dC_z}{di}\infty},$$

with $C_{z_\infty} = C_{z_\lambda} + \delta C_z,$

$$\frac{\delta C_z}{\delta i_{y=0}} = \frac{dC_z}{di}\infty,$$

$$C_{z_\infty} = C_{z_\lambda} + \delta i_{y=0}\frac{dC_z}{di}\infty \quad \text{and} \quad \delta i_{y=0} = A_{ex}\, i_g.$$

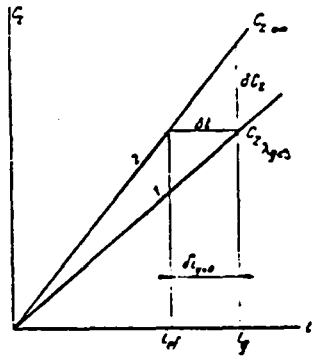

Figure 25

The coefficient A used is the one derived from the measurement performed by Mr. Carafoli:

$$C_{z_\infty} = C_{z_\lambda} + A_{ex}\, i_g \frac{dC_z}{di}\infty.$$

From (10), we derive:

$$C_{z_\infty} = C_{z_\lambda} + A_{ex}\frac{C_z}{\frac{dC_z}{di}\infty}\cdot\frac{dC_z}{di}\infty,$$

$$C_{z_\infty} = C_{z_\lambda} + A_{ex}\, C_{z_\infty} = \frac{C_{z_\lambda}}{1 - A_{ex}}.$$

Thus, the knowledge of the unit lift coefficient of the profile of the median section of a rectangular wing with aspect ratio λ allows one to determine the unit coefficient of lift of the profile under consideration for infinite experimental aspect ratio.

The circulation in the median section of a rectangular wing with aspect ratio λ is equal to

$$\Gamma_0 = C_{z_\lambda}\frac{V_0 l}{2}.$$

The circulation of the edge vortices of the wing can be written as follows according to our hypotheses:

$$\Gamma'_0 = \frac{C_{z_\infty} V_0 l}{2},$$

/46

so that

(11) $$\frac{\Gamma'_0}{\Gamma_0} = \frac{C_{z_\infty}}{C_{z_\lambda}} = \frac{1}{1 - A_{ex}} \text{ from which } \Gamma'_0 = \Gamma_0\left(\frac{1}{1 - A}\right);$$

Therefore, it is not necessary to have the characteristics of the profiles which make up the tested wings in order to find the circulation of the edge vortices.

Rectangular wings

Wings with aspect ratio 5.

Span: 7.62 m (reference [8]).

In plate 16, we show the distribution of the experimental and theoretical lift (Glauert and system 1).

For the calculation of the lift performed by using the system of replacement no. 1, the factor t in formula (7) which has the dimension of a time is determined so that the curve calculated follows the experimental curve as well as possible. For this wing, t is found equal to t = 3500.

Span: 0.90 m (reference [9]).

The experimental and theoretical curves for this wing are shown in plate 17 with t = 31.5.

Remark. Comparison between the experimental lift distributions referred to the same geometric incidence angle of a median profile for these two wings (plate 18) shows deviations between the curves near the edges. This therefore shows that the lift of the extremities of a rectangular wing seems to be related to the geometric dimensions of the wing.

Wing with aspect ratio 3.

Span: 4.56 m (reference [10]).

In plate 19, we show the theoretical and experimental curves for t = 3000.

The agreement between the experimental curve and the one obtained from the system 1 seems to be poorer than for the preceding wings. In any case, the deviations found do not seem to be larger than those obtained between the Glauert curve and the experimental curve.

Rectangular wing with rounded edges

Wing with aspect ratio 6 (reference [11]).

Span: 0.732 m.

Plate 20 shows satisfactory agreement between the curve obtained by using system 1 and the experimental curve t = 27.

Elliptical distribution wing

Wing with aspect ratio 6 (reference [11]).

Span: 1.166 m.

/47

In plate 21 we show the theoretical and experimental curves for this wing t = 209.

We have seen that for a wing with an elliptical distribution of lift along the span, according to the Prandtl theory, the velocity induced is constant along the span and equal to

$$w = \frac{\Gamma_0}{2L},$$
$$\Gamma_0 = C_{z_\infty} \frac{V_0 l_0}{2};$$

for the median section, we have:

$$\frac{w}{V_0} = \frac{i \frac{dC_z}{di}_\infty l_0}{4L}, \qquad \delta i^0_{y=0} = 57{,}3 \frac{i \frac{dC_z}{di}_\infty}{\frac{4L}{l}}, \qquad A_{el} = \frac{\delta i_{y=0}}{i} = \frac{57{,}3 \frac{dC_z}{di}_\infty}{\frac{4L}{l}};$$

the coefficient A derived from our system 1 is equal to:

$$A_1 = \frac{57{,}3 \frac{dC_z}{di} \infty}{6{,}28 \frac{L}{l}},$$

so that the ratio between the coefficients A_{el} and A_1 is equal to:

$$\frac{A_{el}}{A_1} = \frac{4}{6{,}28} = 0{,}64.$$

Remark. Various comparisons made between the curves obtained using our replacement system and experimental curves show that the approximation obtained by using the proposed calculation method is good. At the edge it gives the increase in the lift found in experiments for wings having a rectangular plan form.

In Figure 22, we show the values of the semi-spans of wings proposed as a function of the logarithms of the corresponding t factors. We obtain a curve which has an interpolated part, for which there are no tests in the region of the curve under consideration.

IV. Replacement system no. 2 for a finite span wing

1. Summary of the theory of thin profiles

For a thin profile with a small curvature, it is possible to replace a wing profile by its average line. Over this line the vortex layer is distributed. Let γ be the circulation of an element of this layer with the abscissa x, for which the circulation equals:

$$\gamma = \frac{\partial \Gamma}{\partial s} ds \qquad (\Gamma \text{ circulation around profile})$$

/48

The elementary force at P (Figure 26) is equal to:

$$f ds = \rho V \gamma ds;$$

V, velocity of the point under consideration.

The distribution of the elementary circulations is related to the shape of the average line in the direction of the translation velocity V_o. This distribution is determined by the following geometric condition: The velocity resulting at a point of the average line (velocity coming from the composition of the velocities induced by the vortex elements distributed over the line and the translation velocity V) has to be tangent at any point of the average line.

In order to facilitate the calculations of velocity, induced by the vortex elements, the elementary vortices γ are replaced by their projections on AC so that an element ds of the average line corresponds to a length element dx of the line AC (Figure 26).

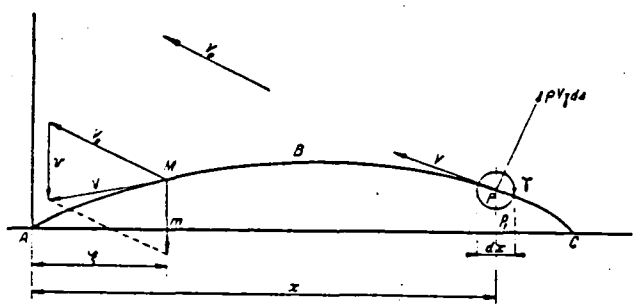

Figure 26

The elementary speed induced in m, projection of M, by the element located at P_1 has the following value:

$$dv = \frac{-\gamma}{2\pi(x-\zeta)} = -\frac{1}{2\pi}\frac{\partial\Gamma}{\partial x}\frac{dx}{x-\zeta}.$$

The total induced velocity in m by elementary vortices distributed over AC is:

$$v = -\frac{1}{2\pi}\int_0^l \frac{\partial\Gamma}{\partial x}\frac{dx}{x-\zeta}.$$

The condition for tangency of the velocity vector at all points of the average line can be written as

$$\frac{v}{V_0} - i = \frac{dy}{dx}. \tag{12}$$

One usually expands the distribution of the circulation along the average profile line (Glauert) in a series in order to calculate v. We then have

$$\frac{\partial \Gamma}{\partial x}\,dx = V_0 l\left[A_0(1-\cos\theta) + \sum_1^\infty A_n \sin n\theta \sin\theta\right] d\theta,$$

with

$$x = \frac{l}{2}(1-\cos\theta),$$

$$v(x) = -V_0\left[A_0 + \sum_1^\infty A_n \cos n\theta\right], \qquad \frac{dy}{dx} = A_0 - i + \sum_1^\infty A_n \cos n\theta.$$

The coefficients $A_0, A_1, \ldots, A_n)$ are equal to

$$A_0 - i = A = \frac{1}{\pi}\int_0^\pi \frac{dy}{dx}\,d\theta, \qquad A_1 = \frac{2}{\pi}\int_0^\pi \frac{dy}{dx}\cos\theta\,d\theta \ldots, \qquad A_n = \frac{2}{\pi}\int_0^\pi \frac{dy}{dx}\cos n\theta\,d\theta.$$

It is therefore possible if we have a given average line to determine the distribution of the elementary circulations along this line and in this way to find the lift of the profile.

Also, if the circulation distribution is according to a selected law, the geometric condition of tangency of velocity vector at any point of the average line will allow one to determine the shape of this line.

2. Action on a thin profile of a vortex located outside of it

a) Action on a circular contour of a vortex located outside of this contour.

Mr. Pistolesi [12] showed that the circulation around a circular contour is modified by a vortex located outside of it. The complementary circulation due to the influence of an exterior vortex on the generating circle of a wing profile is equal to the following product:

$$\Delta\gamma = 4\pi a \Delta v_1,$$

from which:

$$\Delta v_1 = \Delta v \cos\alpha$$

a, is the radius of the generating circle.

The velocity induced can be written as:

$$\Delta v = \frac{\Gamma'_0}{2\pi r};$$

r = the distance of the vortex from the point under consideration. For $\alpha = 0$, we find

$$\Delta\gamma = \frac{4\pi a\Gamma'_0}{2\pi r} = \frac{2a\Gamma'_0}{r};$$

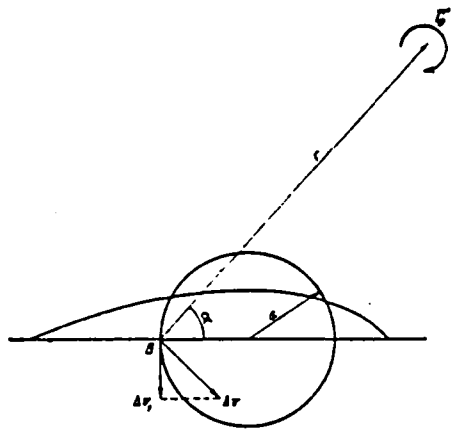

Figure 27

b) Action on the average vortex line of a profile from an outside vortex.

Let us simulate a vortex element γ of the average line into a circle with diameter dx (Figure 28).

/50

Due to the fact that there is a vortex Γ'_0 outside of the profile, the circulation γ of an element is modified by the following amount:

$$\Delta\gamma = 4\pi\frac{dx}{2}\Delta v,$$

with

$$\Delta v = \frac{\Gamma'_0}{2\pi(X-x)}, \qquad \Delta\gamma = 4\pi\frac{dx}{2}\frac{\Gamma'_0}{[2\pi(X-x)]} = \frac{\Gamma'_0 dx}{X-x}.$$

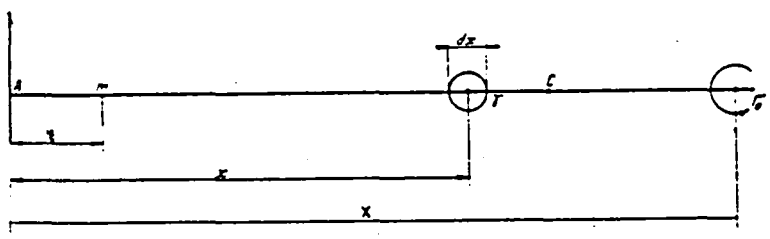

Figure 28

The circulation of the vortex element then becomes

$$\gamma_1 = \gamma + \Delta\gamma,$$

$$\gamma_1 = \gamma = \frac{\Gamma'_0 dx}{X - x} = \frac{\partial \Gamma}{\partial x} dx + \frac{\Gamma'_0 dx}{X - x};$$

and this new elementary circulation can be defined by:

$$\gamma_1 = \frac{\partial \Gamma_1}{\partial x} dx,$$

where Γ_1 is the new distribution of the circulation along the average line of the profile.

The velocity induced by the vortex of intensity γ_1 located at x and induced at point m is equal to:

$$dv' = \frac{-\gamma_1 \cdot}{2\pi(x - \xi)} = -\frac{1}{2\pi} \frac{\partial \Gamma_1 dx}{\partial x (x - \xi)}.$$

The velocity induced at m by vortices distributed over AC is equal to:

$$v' = -\frac{1}{2\pi} \int_0^l \frac{\partial \Gamma_1}{\partial x} \frac{dx}{(x - \xi)}.$$

Finally, one obtains an integral-differential system.

We will use a direct and approximate calculation procedure.

In the replacement system no. 1 for the finite span wing, each profile of the wing operates independently of the adjacent profiles. Its circulation is defined by the resultant of the translation velocity and the velocity induced by the edge vortices.

In analogy with this model, we assume that each vortex element of the average line of a profile will operate independent from adjacent elements.

51

In this way, by considering Figure 29, the complementary induced velocity, induced at m, will have the following value:

$$v_c = -\frac{\Gamma'_0}{2\pi(X - \xi)}.$$

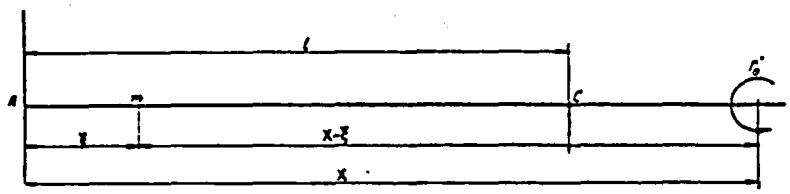

Figure 29

The total induced velocity at m is equal to:

$$v_c + v = v'.$$

The conservation of the shape of the average line of the profile imposes the condition that:

$$\frac{v}{V_0} - i = \frac{dy}{dx} = \frac{v'}{V_0} - i' = \frac{v_c + v}{V_0} - i,$$

$$\frac{v_c}{V_0} = i' - i = \delta i_t.$$

Therefore, it is possible to assimilate the action of a vortex outside of the average line of a profile at a point of the profile into a local variation of the direction of the translation velocity. This corresponds to a curve of the aerodynamic field near the profile.

3. Replacement system no. 2 of the finite span wing (hypothesis)

The real wing is replaced by a lifting surface consisting of vortex strips arranged parallel to the span of the wing. These vortices are "bound" to the wing. The circulation of an elementary vortex varies along the span for variable chord and twisted wings. For rectangular untwisted wings, the circulation of the elementary vortices is constant along the span.

/52

At a given section, the wing profile is replaced by its average line. The vortex elements which make up the attached vortices are distributed over this line in conformance with the theory of thin

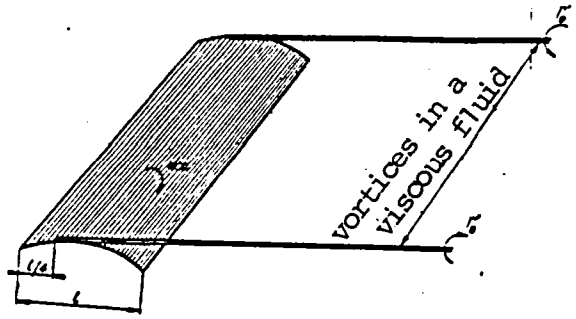

Figure 30

profiles (Figure 30).

At the edges of the wing, the elementary vortices are superimposed in order to create two edge vortices with circulation Γ'_0, and this circulation is defined just like in the case of replacement system no. 1.

The edge vortices have the properties of viscous flow vortices and their origin is fixed at the foci of the profiles of the wing extremities.

4. Calculation of the velocities induced at a point of a finite span wing

The velocity induced at a point A by a vortex element [perfect fluid of length OM and circulation Γ_0 (Figure 31)] is given by the Biot and Savart formula:

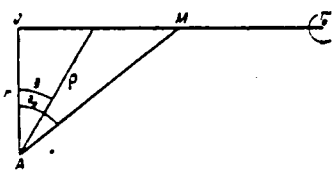

Figure 31

$$v_c = \frac{\Gamma'_0}{4\pi}\int_0^{\theta_0}\frac{d\theta}{\rho}.$$

since $\rho = \frac{r}{\cos\theta}$,

$$v_c = \frac{\Gamma'_0}{4\pi r}\int_0^{\theta_0}\cos\theta\, d\theta = \frac{\Gamma'_0}{4\pi r}\sin\theta_0.$$

Let us consider a rectangular wing (Figure 32). Two edge vortices $\pm\Gamma'_0$ escape from the wing at points M_1 and M_2 such that:

$$M_0M_1 = M'_0M_2 = \frac{l}{4};$$

l = constant cord of the wing.

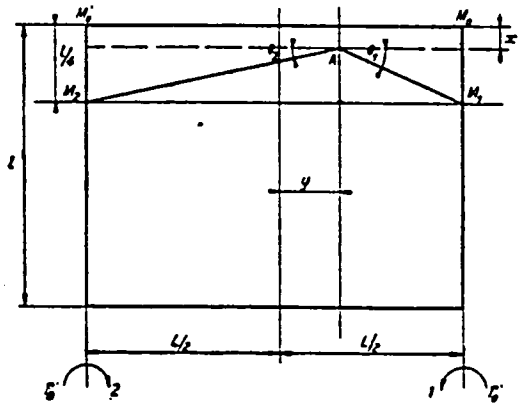

Figure 32

/53

The velocities induced by vortices 1 and 2 (perfect fluid) at the point A whose ordinate is y with respect to the median section of the wing and whose abscissa is x with respect to the leading edge are equal to:

- velocity induced by vortex 1 at A:

$$v_{1c} = \frac{\Gamma'_0}{4\pi\left(\frac{L}{2} - y\right)} \int_{\theta_1}^{\frac{\pi}{2}} \cos\theta \, d\theta = \frac{\Gamma'_0}{4\pi\left(\frac{L}{2} - y\right)} (1 - \sin\theta_1);$$

- velocity induced by vortex 2 at A:

$$v_{2c} = \frac{\Gamma'_0}{4\pi\left(\frac{L}{2} + y\right)} [1 - \sin\theta_2].$$

The resulting induced velocity at A is equal to:

$$v_c = v_{1c} + v_{2c} = \frac{\Gamma'_0}{4\pi\left(\frac{L}{2} + y\right)} [1 - \sin\theta_1] + \frac{\Gamma'_0}{4\pi\left(\frac{L}{2} + y\right)} [1 - \sin\theta_2]$$

$$= \frac{\Gamma'_0}{4\pi} \left\{ \left[\frac{1 - \sin\theta_1}{\frac{L}{2} - y} \right] + \left[\frac{1 - \sin\theta_2}{\frac{L}{2} + y} \right] \right. \tag{13}$$

In particular, for the median section the velocity induced has the following value:

$$v_c = \frac{\Gamma'_0}{\pi L} [1 - \sin\theta_0]. \tag{14}$$

The velocity induced at A by vortices 1 and 2 in a viscous fluid has the following value:

$$v_c = \frac{\Gamma'_0}{4\pi}\left[\left(\frac{1-\sin\theta_1}{\frac{L}{2}-y}\right)\left(1-e^{-\frac{\left(\frac{L}{2}-y\right)^2}{4\nu t}}\right)+\left(\frac{1-\sin\theta_2}{\frac{L}{2}+y}\right)\left(1-e^{-\frac{\left(\frac{L}{2}+y\right)^2}{4\nu t}}\right)\right].$$

It is therefore possible to calculate the resulting induced velocity, induced by edge vortices in a viscous fluid, at any point of a section of a finite span wing.

At one point of a profile, the action of the velocity induced by an outside vortex can be assimilated into a local variation of the translation velocity direction (action on a thin profile of an outside vortex). It has the following value:

$$\frac{v_c}{V_0} = i' - i = \delta i_l.$$

/54

By replacing v_c by its value from (15), we determine the local induced angle which is equal to:

$$(16)\quad \delta i_l = \frac{\Gamma'_0}{4\pi V_0}\left[\left(\frac{1-\sin\theta_1}{\frac{L}{2}-y}\right)\left(1-e^{-\frac{\left(\frac{L}{2}-y\right)^2}{4\nu t}}\right)+\left(\frac{1-\sin\theta_2}{\frac{L}{2}+y}\right)\left(1-e^{-\frac{\left(\frac{L}{2}+y\right)^2}{4\nu t}}\right)\right].$$

In this way, we have defined a local induced angle which varies at all points of a given section of a finite span wing.

The above calculation method allows one to plot diagrams of pressure for sections of finite span wings. In order to plot these diagrams, it is necessary to have profile pressure diagrams which make up the wing, established for experimental infinite aspect ratio and for different incidence angles. In effect, it is then possible to plot $C_p = f(i)$ curves (local pressure coefficient) for infinite experimental aspect ratio. Let (Figure 33) us consider the curve obtained in this way for a point with abscissa x. When the profile

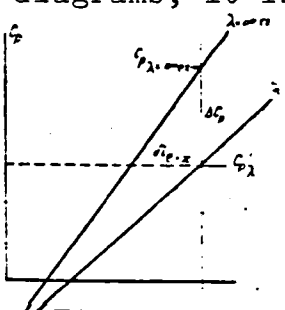

Figure 33

corresponds to a wing with aspect ratio λ at the point under consideration, there exists an induced angle $\delta i_{l=x}$ to which corresponds a pressure coefficient variation ΔC_p such that:

$$\frac{\Delta C_p}{\delta i_{l=x}} = \frac{dC_{p_{\lambda=\infty_{ex}}}}{di}, \qquad \Delta C_p = \frac{dC_{p_{\lambda=\infty_{ex}}}}{di} \delta i_{l=x}.$$

The value of the pressure coefficient at the point being studied and for aspect ratio λ is therefore equal to:

$$C_{p_{\lambda=\infty_{ex}}} - \Delta C_p = C_{p_\lambda}.$$

From $C_{\lambda=\infty_{ex}} = f(i)$, curves, one can determine the characteristics $C_{p_\lambda} = f(i)$ (aspect ratio λ) which allows one to find pressures at any point of finite span wings.

5. Experimental verifications

Mr. Carafoli measured pressures in the median section of wings with various aspect ratios which varied between 2 and 8. He also made measurements in the median section of a wing placed between panels. Among these experiments, we only used the results of the tests with the aspect ratio two wing and the wing between panels. We believe that the selection of aspect ratio 2 was justified because of the fact that the curvature of the aerodynamic field increases when the aspect ratio decreases. We made the selection to verify our replacement system.

We plotted experimental curves $C_p = f(i)$ for various measurement points (aspect ratios 2 and $\lambda = \infty_{ex}$).

/55

In the following table we show data on the sides of the profiles used by Mr. Carafoli and shown in Figure 34. The pressure tap orifices were located at the points which serve to construct the wing profile (sides given in percentage of the chord):

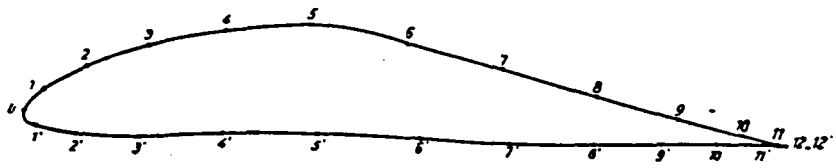

Figure 34

	0	1	2	3	4	5	6	7	8	9	10	11	12
x	99,80	97,50	92,00	84,00	74,00	62,50	49,75	37,30	24,55	13,80	5,66	0,80	~ 0
y	9,03	11,80	15,04	17,92	19,80	20,05	18,40	15,66	12,40	9,78	7,65	6,52	6,76

	0	1'	2'	3'	4'	5'	6'	7'	8'	9'	10'	11'	12'
x	99,80	98,35	93,25	85,00	73,80	61,51	48,00	36,00	25,35	16,25	8,65	2,89	0
y	9,03	6,89	5,96	6,15	6,47	6,65	6,27	5,89	5,77	6,27	6,52	6,82	6,76

In formula (16), the calculation shows that for the median section of the wings tested, the term which takes into account the fluid viscosity can be ignored.

We calculated the local induced angles (median section) along the chord of a wing with aspect ratio 2 for various incidences. We then related the $C_{p_\lambda} = f(i)$ experimental curves for aspect ratio 2 with those for the infinite experimental ratio curves.

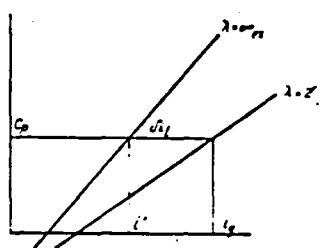

Figure 35

For this purpose, let us consider Figure 35. Knowledge of the $C_{p_\lambda} = f(i)$ ($\lambda = 2$) curve allows one to determine δi_1 for aspect ratio λ by calculating the angle induced at the point under consideration for a given geometric incidence. Therefore, we find an aerodynamic operational incidence i' at the point under study equal to:

$$i' = i_g - \delta i_i.$$

Using the Glauert method, we calculated the induced angles for the median profile of a wing with an aspect ratio of $\lambda = 2$ and for various geometric incidences.

In plates 23 to 28, we show the $C_p = f(i)$ curves for $\lambda = 2$ and $\lambda = \infty_{ex}$ as well as the curves which one obtains by reducing those for $\lambda = 2$ to $\lambda = \infty_{ex}$ either using the Gauert method or by using our system no. 2.

In his thesis, Mr. Carafoli also gives values of induced angles corresponding to his measurements (determined from $C_z = f(i)$ curves for median sections of tested wings). By using these experimental induced angles and by using Figure 35, we plotted $C_p = f(i_g - \delta i_l)$ which are shown in plates 25 and 26.

/56

In plate 29, we show pressure diagrams for the median wing sections. One wing is between panels (infinite experimental aspect ratio) and the other is for the aspect ratio 2, reduced to $\lambda = \infty_{ex}$ using the Glauert method and using our system 2. The agreement obtained between the experimental curve and the one derived from system 2 is satisfactory.

V. Use of the replacement system no. 2 for the study of the influence of lateral boundary layers on tests between panels

1. Hypotheses

The hypotheses introduced in Chapter II for finding the influence of lateral boundary layers on tests between panels allow one to determine the unit lift coefficients of the profiles under study. For the same effective incidence (median profile) and for a wing with a large geometric aspect ratio and for a wing with a reduced geometric aspect ratio in a plane flow, substantial differences were found between the various pressure diagrams measured under these experimental conditions. It seemed to us to be possible to adapt the

replacement system no. 2 to plane flow tests in order to reduce the deviations among the various diagrams.

The wing placed in a plane flow traverses the wind tunnel without a lateral play. It has a constant profile and chord and is not twisted.

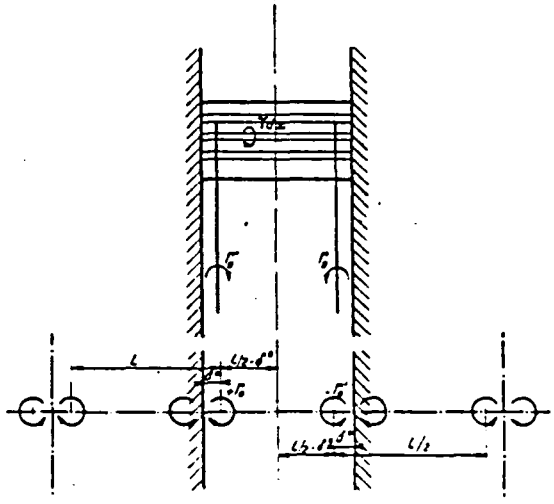

Figure 36

This wing is replaced by elementary vortices with constant circulation arranged parallel to the span and having the same transverse dimensions as the real wing.

/57

In a section the base profile is replaced by its average line. The elementary vortices are distributed over this line (real thin profiles).

At the edges of the wing, the elementary vortices superimpose and generate two vortices in a viscous fluid which come from the wing at the foci of the profile located at the displacement thickness of the lateral boundary layers which develop along the walls of the wind tunnel. These extend to the foci considered to be at infinity downstream (Figure 36) (viscosity is only involved near the vortex axes).

The circulation of the edge vortices is defined in systems 1 and 2.

The flow is produced between the walls and it is necessary to take into account the stresses which affect the fluid caused by the walls. These stresses are represented by image vortices. Figure 36 gives the diagram of the equivalent vortex system.

This is an infinite row of semi-vortices with alternate orientations with circulation $\pm\Gamma'_0$ and step L and with the following origin abscissa:

$$y = \pm\left(\frac{L}{2} - \delta^*\right).$$

2. Calculation of induced velocity

The velocity induced at a ordinate point Y by two vortices in perfect fluid with circulation $\pm\Gamma'_0$ of step L and located at a distance y from the wind tunnel axis is equal to:

$$v_c = \frac{\Gamma'_0}{2L}\frac{\sin\frac{2\pi y}{L}}{\cos\frac{2\pi y}{L} - \cos\frac{2\pi Y}{L}},$$

with

$$y = \frac{L}{2} - \delta^*, \qquad v_c = \frac{\Gamma'_0}{2L}\frac{\sin\frac{2\pi\left(\frac{L}{2}-\delta^*\right)}{L}}{\cos\frac{2\pi\left(\frac{L}{2}-\delta^*\right)}{L} - \cos\frac{2\pi Y}{L}};$$

in particular, for the median section, we have:

$$v_c = \frac{\Gamma'_0}{2L}\frac{\sin\frac{2\pi y}{L}}{\cos\frac{2\pi y}{L} - 1} = \frac{\Gamma'_0}{2L}\frac{\sin\frac{2\pi}{L}\left(\frac{L}{2}-\delta^*\right)}{\cos\frac{2\pi}{L}\left(\frac{L}{2}-\delta^*\right) - 1}.$$

Let us consider Figure 37. The vortices $\pm\Gamma'_0$ are located at a distance of δ^* from the wall which is small in most cases. The velocity induced in the median section is practically due to the vortices themselves and their first image. It is possible to locate two fictitious vortices at PP' along the extremities of the wing and whose circulation $\pm\Gamma'_0$ is defined so that the velocity induced at A

(focus of the profile of the median section) by these vortices is identical with the one induced at the same point by the vortices $\pm\Gamma'_0$ and their images: /58

$$v_{c_A} = \frac{2\Gamma''_0}{4\pi}\left(\frac{1}{\frac{L}{2}}\right) = \frac{\Gamma'_0}{2L}\frac{\sin\frac{2\pi}{L}\left(\frac{L}{2}-\delta^*\right)}{\cos\frac{2\pi}{L}\left(\frac{L}{2}-\delta^*\right)-1},$$

$$v_{c_A} = \frac{\Gamma''_0}{\pi L} = \frac{\Gamma'_0}{2L}\frac{\sin\frac{2\pi}{L}\left(\frac{L}{2}-\delta^*\right)}{\cos\frac{2\pi}{L}\left(\frac{L}{2}-\delta_*\right)-1},$$

$$\Gamma'' = \frac{\pi}{2}\Gamma'_0\frac{\sin\frac{2\pi}{L}\left(\frac{L}{2}-\delta^*\right)}{\cos\frac{2\pi}{L}\left(\frac{L}{2}-\delta^*\right)-1}.$$

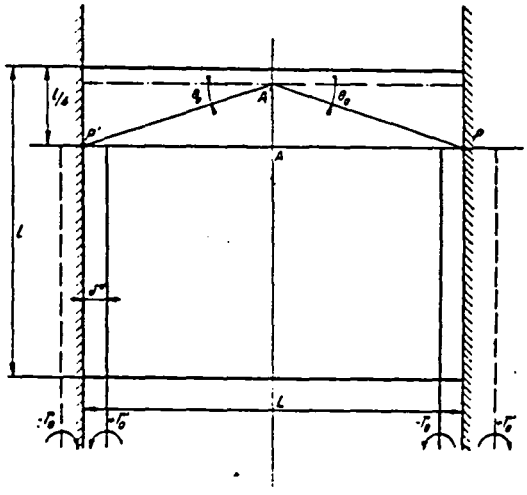

Figure 37

We can therefore replace the wing between panels by a finite span wing (L) and one can calculate the velocity induced by the edge vortices of circulation $\pm\Gamma'_0$ at any point of the median section using replacement system no. 2.

In particular, the velocity induced at A' (Figure 37) is equal to:

$$v_{c_{A'}} = \frac{\Gamma''_0}{4\pi L}(1 - \sin\theta_0).$$

and by replacing Γ'' by its value:

$$v_{c_{A'}} = \frac{\Gamma'_0}{2L}\frac{\sin\frac{2\pi}{L}\left(\frac{L}{2} - \delta^*\right)}{\cos\frac{2\pi}{L}\left(\frac{L}{2} - \delta^*\right) - 1}(1 - \sin\theta_0);$$

In this way one can calculate the induced angle at any point of the median section of a wing between panels. At the point A', it has the following value: /59

$$\delta i_{l=A'} = \frac{\Gamma'_0}{2LV_0}\left[\frac{\sin\frac{2\pi}{L}\left(\frac{L}{2} - \delta^*\right)}{\cos\frac{2\pi}{L}\left(\frac{L}{2} - \delta^*\right) - 1}(1 - \sin\theta_0)\right]$$

$$= \frac{\Gamma'_0}{2LV_0}\left[\frac{\sin 2\left(\frac{\pi}{2} - \frac{\pi\delta^*}{L}\right)}{\cos 2\left(\frac{\pi}{2} - \frac{\pi\delta^*}{L}\right) - 1}(1 - \sin\theta_0)\right]$$

$$= \frac{\Gamma'_0}{2LV_0}\left[\frac{2\sin\left(\frac{\pi}{2} - \frac{\pi\delta^*}{L}\right)\cos\left(\frac{\pi}{2} - \frac{\pi\delta^*}{L}\right)}{-2\sin^2\left(\frac{\pi}{2} - \frac{\pi\delta^*}{L}\right)}(1 - \sin\theta_0)\right],$$

(17)

$$\delta i_{l=A'} = \frac{\Gamma'_0}{2LV_0}\left[-\operatorname{cotg}\left(\frac{\pi}{2} - \frac{\pi\delta^*}{L}\right)(1 - \sin\theta_0)\right]$$

$$= -\frac{\Gamma'_0}{2LV_0}\operatorname{tg}\frac{\pi\delta^*}{L}(1 - \sin\theta_0).$$

3. Experimental verifications

We performed pressure measurements in median sections of wings in a plane flow with geometric aspect ratios of $\lambda_g = 0.55$ and $\lambda_g = 8.6$ (tests described in Chapter II). The tests performed with $\lambda_g = 8.6$ can be considered as corresponding to a wing with infinite experimental aspect ratio. We plotted the curve $C_p = f(i)$ for aspect ratios $\lambda_g = 8.6$ and $\lambda_g = 0.55$ for various pressure tap orifices located on the top side and the bottom side of the profile.

We calculated the angle induced at these points by using system no. 2 of replacement for the finite span wing adapted to the plane flow tests for various values of the geometric incidence angle of the wing. We then plotted $Cp_\lambda = f(i_g - \delta i_l)$ curves for the aspect ratio $\lambda_g = 0.56$. These curves are very close to the ones obtained for the infinite experimental aspect ratio.

The sides of the measurement points are represented in the following table:

N°	1	2	3	4	5	6	7	8	9	10
x	0	2 mm	6,1 mm	11,6 mm	22 mm	30,4 mm	40,5 mm	51,6 mm	62,2 mm	73 mm
y	4,6 mm	8,6 mm	11,8 mm	14,2 mm	16,2 mm	16,2 mm	15,4 mm	13,2 mm	10,8 mm	7 mm

N°	11	12	13	14	15	16	17	18	19	
x	82,4 mm	80	70,5	59,5	47,6	35,7	23,8	14	4,5	
y	3,7 mm	0	0	0	0	0	0	0,5	1	

The curves $C_p = f(i)$ are shown in plates 30 to 34. /60

For a given value of the geometric incidence for a wing with aspect ratio [$\lambda_g = 0.55$ (0 incidence)] (Figure 38) and for a given value of the coefficient C_p, the deviation betweeen the experimental $C_p = f(i)$ curve for wings having aspect ratios $\lambda_g = 8.6$ and $\lambda_g = 0.55$ represents the value of the local experimental induced angle at the measurement point considered.

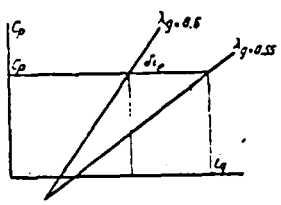

Figure 38

In plate 35, we show the variation of the experimental and theoretical local induced angles [derived from formula (17)] along the wing chord.

The unit lift curves of the profile determined from pressure measurements in the median section of wings having aspect ratios of

$\lambda_g = 8.6$ and $\lambda_g = 0.55$ are shown in plate 4. For the geometric incidence angle $i_g = 0$, the effective experimental induced angle is found to be equal to 2°. We show this value in plate 35.

Finally, in plate 36 we show the pressure diagrams found in the median section of wings with aspect ratios of $\lambda_g = 8.6$ and 0.55 (geometric incidence) as well as the diagram obtained from the one for an aspect ratio of $\lambda_g = 0.55$ and reduced to the infinite experimental aspect ratio using system no. 2. In this plate we also show the pressure diagram measured for the aspect ratio $\lambda_g = 0.55$ and reduced to an infinite experimental aspect ratio, taking into account the effective induced angle for the section under consideration [angle derived from the $C_z = f(i)$ curves]

The agreement between the experimental diagram measured for $\lambda_g = 8.6$, $\lambda_m = \infty$, and the one obtained from $\lambda_g = 0.55$ reduced to the infinite experimental aspect ratio and by using system no. 2 seems to be good.

Conclusions

The two finite span wing replacement systems proposed seem to give good results compared with experiments, as far as the distribution of lift along the span and the distribution of the pressure along a given section of the wing are concerned (for finite span or between panels). Therefore, it is possible to follow, more precisely than using the Prandtl model, the aerodynamic local operation of a wing. This will allow one to develop a simple replacement model for a propeller.

In more general terms, the Prandtl replacement system agrees with the Helmoltz law about vortices and disagrees with experience because of the existence of a free vortex sheet. It is difficult to imagine the rolling up of the edge vortices. Our replacement systems on the other hand seem to agree well with experimental data

and disagrees with the Helmoltz laws.

On this topic, it should be noted that the edge vortices of a finite span wing violate the fourth theorem of Helmoltz about the constant intensity of the vortices.

/61

A more detailed study on the formation of the edge vortex of the wing as well as its deterioration due to viscosity would be necessary to derive more exact laws than the ones discussed in this chapter. In particular, the correction term which involves the ambient fluid viscosity which we have adopted certainly will not only be the function of the geometric wing dimensions.

End of Document